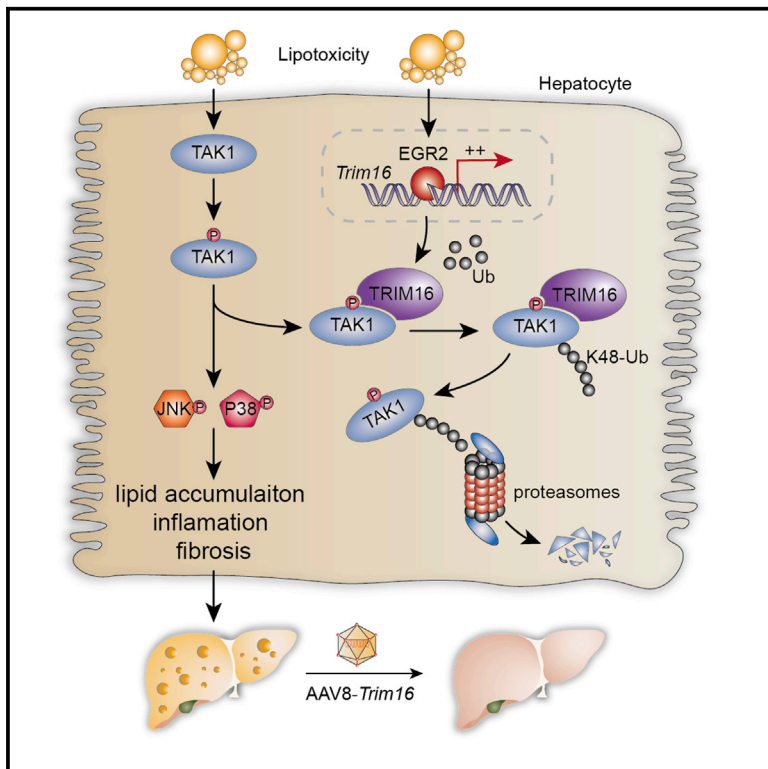# Tripartite motif 16 ameliorates nonalcoholic steatohepatitis by promoting the degradation of phospho-TAK1

Graphical abstract

Authors

Lin Wang, Xin Zhang, Zhi-Bin Lin, ..., Kai-Shan Tao, Hua Han, Ke-Feng Dou

Correspondence

fierywang@163.com (L.W.), doukef@fmmu.edu.cn (K.-F.D.)

In brief

Wang et al. report that TRIM16 ameliorates lipid accumulation and inflammation during NASH progression by facilitating the ubiquitination-dependent degradation of phospho-TAK1. Further, they show that overexpressing TRIM16 in a mouse model of NASH ameliorates pathology.

Highlights

- TRIM16 is transcriptionally activated by EGR2 in response to lipotoxicity

- TRIM16 ameliorates lipid accumulation and inflammation during NASH progression

- TRIM16 inhibits the JNK/p38 pathway by catalyzing ubiquitin-mediated degradation of pTAK1

- AAV8-mediated TRIM16 overexpression attenuates NASH progression in HFHC-fed mice

CellPress

Cell Metabolism

CellPress

Article

Tripartite motif 16 ameliorates nonalcoholic steatohepatitis by promoting the degradation of phospho-TAK1

Lin Wang,[1,5,6,*] Xin Zhang,[2,5] Zhi-Bin Lin,[1,5] Pei-Jun Yang,[1,5] Hao Xu,[1] Juan-Li Duan,[1] Bai Ruan,[1] Ping Song,[1] Jing-Jing Liu,[1] Zhen-Sheng Yue,[1] Zhi-Qiang Fang,[1] Heng Hu,[3] Zhen Liu,[3] Xiao-Li Huang,[3] Ling Yang,[3] Song Tian,[3] Kai-Shan Tao,[1] Hua Han,[1,4] and Ke-Feng Dou[1,*]

[1]Department of Hepatobiliary Surgery, Xi-Jing Hospital, Fourth Military Medical University, Xi'an 710032, China
[2]Department of Gastroenterology, Wuhan Third Hospital, Tongren Hospital of Wuhan University, Wuhan 430000, China
[3]Department of Cardiology, Renmin Hospital of Wuhan University, Wuhan 430000, China
[4]State Key Laboratory of Cancer Biology, Department of Medical Genetics and Developmental Biology, Fourth Military Medical University, Xi'an 710032, China
[5]These authors contributed equally
[6]Lead contact
*Correspondence: fierywang@163.com (L.W.), doukef@fmmu.edu.cn (K.-F.D.)
https://doi.org/10.1016/j.cmet.2021.05.019

SUMMARY

Nonalcoholic steatohepatitis (NASH)-related hepatocellular carcinoma and liver disorders have become the leading causes for the need of liver transplantation in developed countries. Lipotoxicity plays a central role in NASH progression by causing endoplasmic reticulum stress and disrupting protein homeostasis. To identify key molecules that mitigate the detrimental consequences of lipotoxicity, we performed integrative multiomics analysis and identified the E3 ligase tripartite motif 16 (TRIM16) as a candidate molecule. In particular, we found that lipid accumulation and inflammation in a mouse NASH model is mitigated by TRIM16 overexpression but aggravated by its depletion. Multiomics analysis showed that TRIM16 suppressed NASH progression by attenuating the activation of the mitogen-activated protein kinase (MAPK) signaling pathway; specifically, by preferentially interacting with phospho-TAK1 to promote its degradation. Together, these results identify TRIM16 as a promising therapeutic target for the treatment of NASH.

INTRODUCTION

Nonalcoholic fatty liver disease (NAFLD) is the most common cause of chronic liver disease worldwide, especially in developed countries (Sanyal, 2019; Younossi et al., 2019). Without an effective treatment, NAFLD may progress to nonalcoholic steatohepatitis (NASH), which may subsequently lead to hepatocellular carcinoma and a series of metabolic disorders (Wree et al., 2013; Younossi et al., 2016). Over the last few decades, NASH has become the leading cause for the need of liver transplantation in the USA (Noureddin et al., 2018). Although many studies aimed at unraveling the etiology of NAFLD have been conducted, no pharmacotherapies have yet to be approved (Chen et al., 2019b). Thus, there is an urgent need to explore the underlying mechanisms of NASH progression to identify potential molecular targets for its treatment.

Lipotoxicity, a result of excessive accumulation of lipids, is a principal factor in the etiology of NASH (Schuster et al., 2018). Increased lipotoxicity in hepatocytes leads to various deleterious effects, including the aberrant activation of intracellular adaptors and kinases (Schuster et al., 2018), which are known to transmit and amplify upstream signals (Dar and Shokat, 2011). When

abnormally activated, they can trigger downstream signaling cascades that can ultimately lead to cell injury or death (Cai et al., 2019; Xu et al., 2019). Therefore, strategies aimed at inhibiting the extensive activation of pivotal adaptors and kinases have emerged as potential ways to decelerate NASH progression (Arab et al., 2018). The ubiquitin-proteasome system extensively mediates protein stability and function in biological processes (Wu et al., 2020a, 2020b). Hence, it is constructive to discover key ubiquitination-related modulators that can control NASH progression. To fulfill this aim, we conducted RNA sequencing (RNA-seq) of a cell-based model of hepatocyte lipotoxicity and searched for ubiquitination-related molecules in the differentially expressed genes. This approach led to the E3 ligase tripartite motif 16 (TRIM16).

TRIM16 belongs to the TRIM protein family (Jefferies et al., 2011; Joazeiro and Weissman, 2000; Nisole et al., 2005). TRIM proteins are a group of really interesting-new-gene-(RING) domain-containing E3 ligases that exert multiple functions in cell biology and immunity (Jefferies et al., 2011). However, TRIM16, without a classic RING domain, exerts its ubiquitination function via the B box domain instead (Bell et al., 2012). As an E3 ligase, TRIM16 regulates autophagy by promoting the ubiquitination of key regulators in this pathway to maintain cell
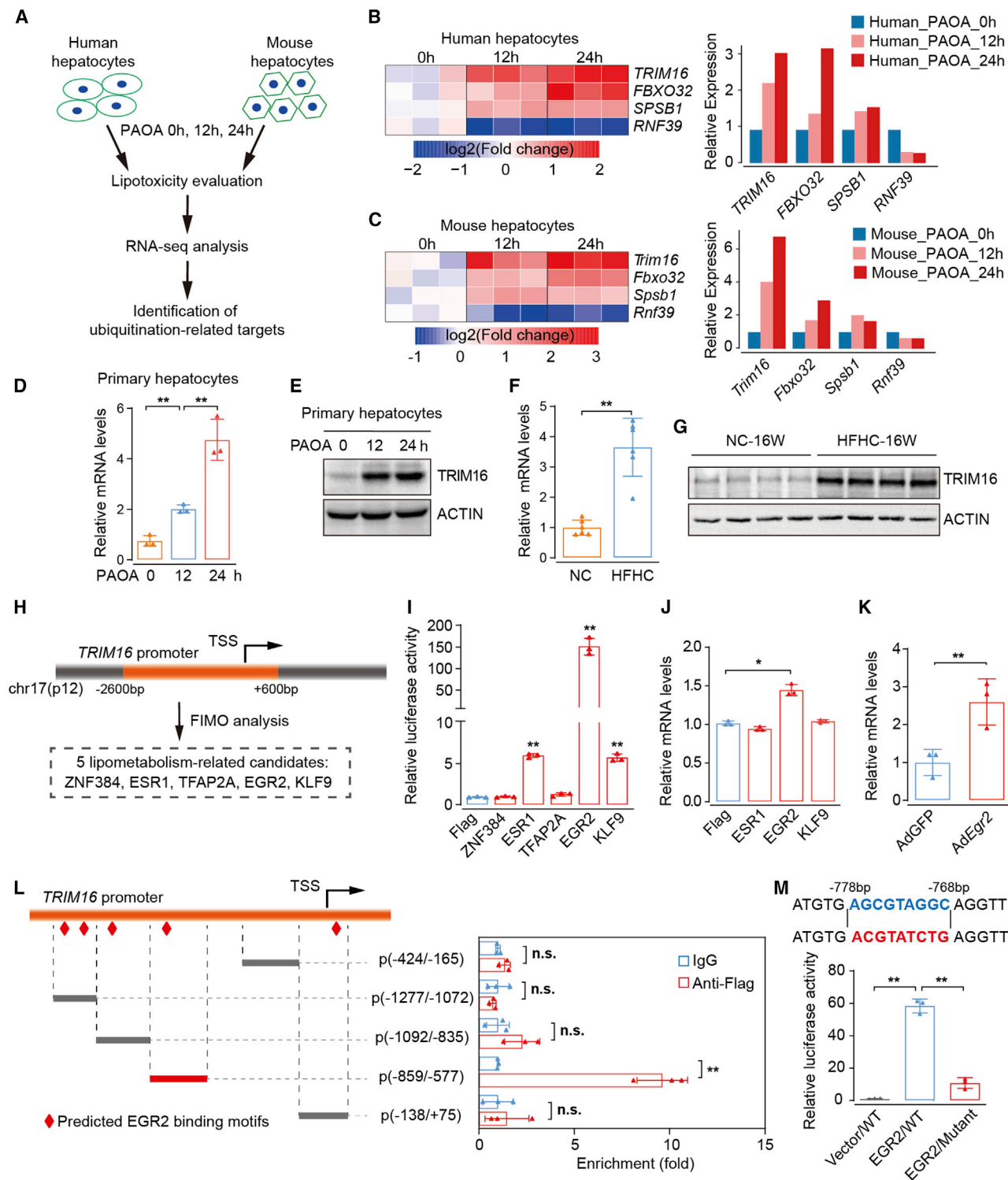
Figure 1. TRIM16 expression is induced by lipotoxicity in hepatocytes

(A) Scheme showing the procedure of identifying ubiquitination-related targets in response to PAOA treatment.

(B and C) Heatmaps showing four differentially expressed ubiquitin-related genes in L02 hepatocytes (B) and mouse primary hepatocytes (C) with PAOA treatment for 12 h and 24 h (1 technical replicate of 3 biological replicates for each group). The right histograms summarize the relative mRNA expression of the four ubiquitin-related genes in the indicated groups.

(D) Relative mRNA levels of TRIM16 in mouse primary hepatocytes in the indicated groups (3 technical replicate of 3 biological replicates for each group).

Cell Metabolism
Article

CellPress

homeostasis (Chauhan et al., 2016; Fraiberg and Elazar, 2016; Jena et al., 2018). TRIM16 also inhibits the malignant behaviors of various tumors through ubiquitination (Cheung et al., 2012; Kim et al., 2016; Marshall et al., 2010). Furthermore, TRIM16 can regulate keratinocyte differentiation and IL-1β secretion (Beer et al., 2002; Munding et al., 2006). However, to the best of our knowledge, no prior study has reported the role of TRIM16 in NASH progression.

In this study, we show that TRIM16 is markedly upregulated in response to lipotoxicity and that it mitigates hepatic steatosis, inflammation, and fibrogenesis in both high-fat diet (HFD)- and high fat and high cholesterol (HFHC)-diet-induced NAFLD models in mice. Mechanistically, we show that TRIM16 attenuates the activation of the mitogen-activated protein kinase (MAPK) signaling pathway, by preferentially interacting with phosphorylated TGF-β-activated kinase 1 (TAK1) and promoting its degradation by catalyzing K48-linked ubiquitination. Moreover, we show that adeno-associated-virus-8-mediated TRIM16 overexpression ameliorates steatohepatitis and liver injury in mice, whereas its deletion worsens such pathology. Collectively, our study suggests that TRIM16 is a specific TAK1 regulator that can be targeted in NASH.

RESULTS

TRIM16 expression is induced by lipotoxicity in hepatocytes

To identify ubiquitination-associated candidate molecules that might stabilize the aberrantly activated kinases induced by lipotoxicity, we performed RNA-seq of a lipotoxic cell-based model, which consisted of L02 human hepatocytes or mouse primary hepatocytes treated with palmitic acid and oleic acid (PAOA) for 12 or 24 h, respectively (Figure 1A) (Moravcová et al., 2015; Ricchi et al., 2009). Lipids and lactate dehydrogenase (LDH) were accumulated in PAOA-treated hepatocytes in a time-dependent manner (Figures S1A and S1B). Thereafter, we performed RNA-seq using hepatocytes treated with PAOA for different time periods. Gene set enrichment analysis (GSEA) revealed that PAOA treatment activated the signaling pathways associated with cell death and inflammation (Figures S1C and S1D), indicating the successful

inducement of lipotoxicity in the treated hepatocytes. Subsequently, we analyzed differentially expressed genes (DEGs), which were either upregulated or downregulated in the two species of hepatocytes with PAOA treatment for 12 and 24 h. A full description of the criteria of the screen is detailed in the STAR methods. We noted that four E3 ligases met the criteria of the screen; namely, TRIM16, FBXO32, SPSB1, and RNF39, among which TRIM16 presented the greatest expression alteration (Figures 1B and 1C). To verify the RNA-seq results, we performed qPCR analyses and found that TRIM16 mRNA markedly increased in a time-dependent manner in PAOA-treated L02 and primary hepatocytes (Figures 1D and S1E). Moreover, TRIM16 protein was markedly induced in the lipotoxic-cell-based model (Figures 1E and S1F). Similarly, the mRNA and protein expression of TRIM16 were enhanced in mice, after 24 weeks of HFD feeding or 16 weeks of HFHC feeding (Figures 1F, 1G, S1G, and S1H). The intensified TRIM16 expression was also confirmed in the livers of individuals with NASH compared with those without NASH (Figure S1I). Overall, TRIM16 was upregulated in the setting of lipotoxicity.

To explore how lipotoxicity induces TRIM16 expression, we predicted the identity of TRIM16-promoter-binding transcription factors (TFs) by using the FIMOs (find individual motif occurrences) tool; by this manner five candidate TFs (ZNF384, ESR1, TFAP2A, EGR2, and KLF9) were identified (Figure 1H). Then, luciferase plasmids that contained the full TRIM16 promoter region (−2,600 ~ +600 bp) or truncated versions were constructed, and dual-luciferase report assays were conducted (see the STAR methods for details of the constructs developed). We found that EGR2, ESR1, and KLF9 could induce the activation of the full TRIM16 promoter, with EGR2 possessing the highest change fold (Figure 1I). Whereas in L02 hepatocytes treated with PAOA, only EGR2 overexpression activated the transcription of TRIM16 (Figure 1J). Consistent with these results, qPCR analysis confirmed TRIM16 upregulation in AdEgr2-infected primary hepatocytes (Figure 1K), indicating that EGR2 was the most probable TF regulating TRIM16 expression. To verify this regulation, we designed primers that amplified the regions containing the EGR2 binding sites predicted by the FIMO tool and performed a chromatin immunoprecipitation (ChIP) assay (Figure 1L). We found that

(E) Representative western blot image showing TRIM16 protein levels in mouse primary hepatocytes in the indicated groups (1 technical replicate of 3 biological replicates for each group).

(F) Relative mRNA levels of TRIM16 in the livers of HFHC-fed mice and the negative control mice (3 technical replicate of 6 biological replicates for each group).

(G) Representative western blot image showing TRIM16 protein levels in the livers of the mice in the indicated groups (1 technical replicate of 4 biological replicates for each group).

(H) Prediction of TRIM16-promoter-binding TFs by FIMO software (version 4.10.2) and literature analyses. TSS, transcription start site.

(I) Relative luciferase activity of the luciferase reporter plasmid containing TRIM16 promoter in L02 hepatocytes transfected with the plasmids overexpressing the five predicted transcription factors and the control plasmid, and then treated with PAOA for 12 h (3 technical replicate of 3 biological replicates for each group).

(J) Relative mRNA levels of TRIM16 in L02 hepatocytes transfected with the indicated plasmids after treated with PAOA for 12 h (3 technical replicate of 3 biological replicates for each group).

(K) Relative mRNA levels of TRIM16 in AdEgr2- or AdGFP-infected mouse primary hepatocytes after PAOA treatment for 12 h (3 technical replicate of 3 biological replicates for each group).

(L) Relative enrichment of Flag-EGR2 on the indicated regions of TRIM16 promoter in L02 hepatocytes detected by ChIP assay using anti-Flag or control IgG antibody, combined with qPCR assay (3 technical replicate of 3 biological replicates for each group).

(M) Relative luciferase activity of luciferase reporter plasmids containing wild-type TRIM16 promoter (WT) or its mutant in L02 hepatocytes transfected with the plasmids overexpressing EGR2 or the control plasmid, and then treated with PAOA for 12 h (n = 3 independent experiments per group). The upper sequences show EGR2 binding motif (blue) and its mutant (red) (3 technical replicate of 3 biological replicates for each group).

In all statistical plots, data are expressed as the mean ± SD, *p < 0.05, **p < 0.01; n.s., not significant. For (D), (I), (J), (L), and (M), statistical analyses were carried out by one-way ANOVA with Bonferroni post hoc analysis for data meeting homogeneity of variance requirements or Tamhane's T2(M) post hoc analysis for heteroscedastic data. For (F) and (K), statistical analyses were carried out by two-tailed Student's t test. Gene expressions were normalized ACTB. See also Figures S1 and S2 and Tables S1, S2, and S7.
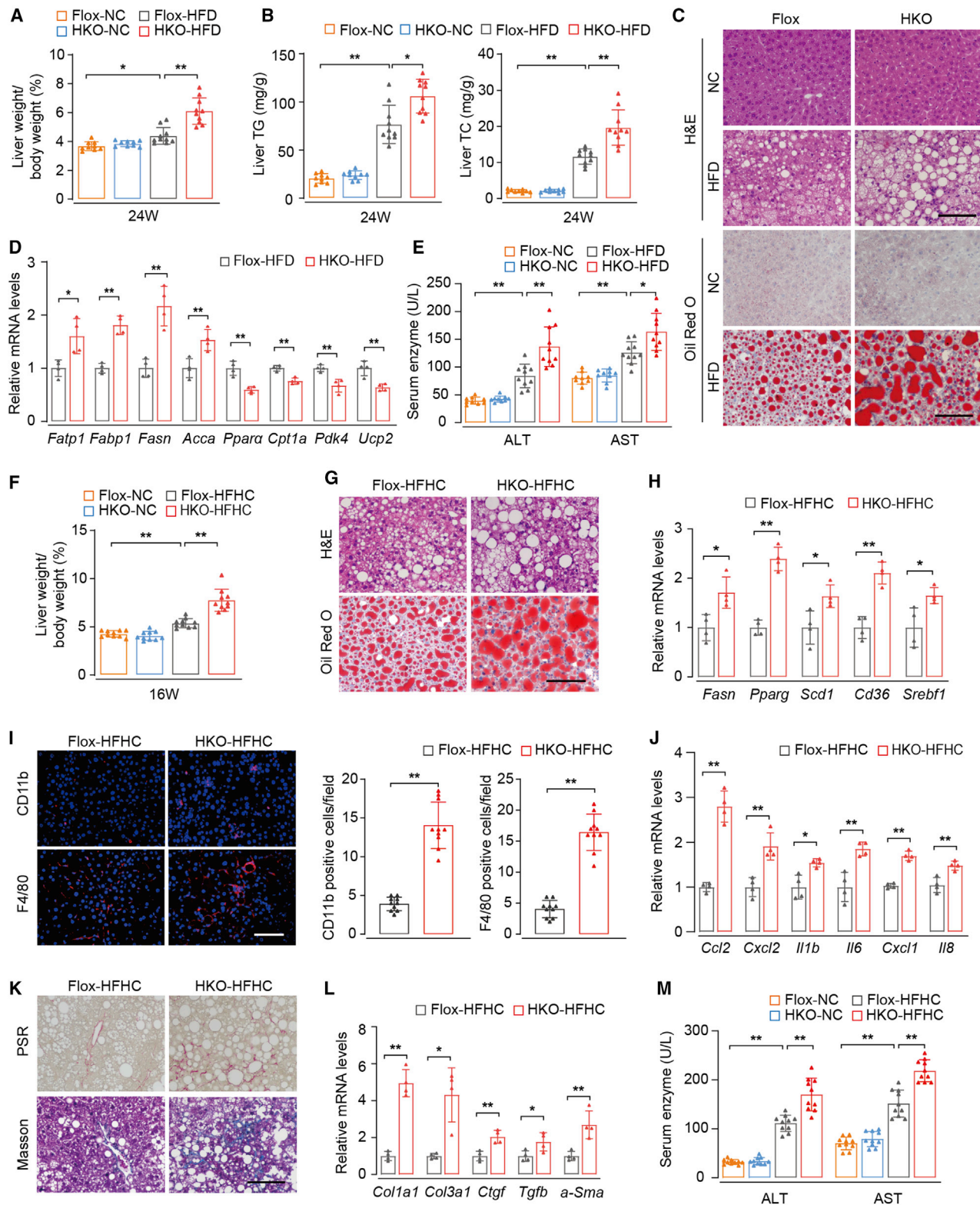
Figure 2. Hepatocyte-specific TRIM16 deletion exacerbates HFD- and HFHC-induced hepatic injury

(A) Ratios of liver weight to body weight of *Trim16*-HKO mice and their corresponding controls *Trim16*-Flox mice after NC or HFD consumption for 24 weeks (1 technical replicate of 9–10 biological replicates for each group).

(B) Hepatic TG and TC contents of the mice in the indicated group (3 technical replicate of 9–10 biological replicates for each group).

(legend continued on next page)

Cell Metabolism
Article

CellPress

EGR2 directly bound to the TRIM16 promoter at −859 ∼ −577 bp; moreover, mutation of the predicted binding site (−778 ∼ −768 bp) in this region significantly inhibited the effect of EGR2 on TRIM16 promoter activation (Figure 1M).

TRIM16 inhibits lipotoxicity-induced lipid accumulation and inflammation

To investigate the function of TRIM16 in the setting of lipotoxicity, primary hepatocytes were infected with *Trim16*-overexpressing adenovirus (Ad*Trim16*) or a control AdGFP and then treated with PAOA. Western blot and qPCR analyses confirmed TRIM16 overexpression in Ad*Trim16*-infected hepatocytes (Figures S2A and S2B). Nile red staining indicated that Ad*Trim16* attenuated aberrant lipid accumulation in PAOA-treated hepatocytes compared with the control group (Figure S2C). Similarly, TRIM16 overexpression in PAOA-treated primary hepatocytes markedly ameliorated the increase in triglyceride (TG) and total cholesterol (TC) concentrations (Figure S2D).

Next, we conducted RNA-seq to determine the alteration of the transcriptional profile in Ad*Trim16*-infected hepatocytes. Hierarchical clustering analysis revealed that the gene expression profiles in AdGFP-PAOA and Ad*Trim16*-PAOA cells were clearly separated (Figure S2E). GSEA revealed that pathways related to lipogenesis, inflammation, and apoptosis were downregulated by TRIM16 overexpression (Figure S2F), which was further confirmed by qPCR (Figure S2G). Conversely, adenovirus-vector-mediated TRIM16 knockdown (Adsh*Trim16*) aggravated lipid accumulation, TG/TC concentration, and proinflammatory gene expression in PAOA-treated hepatocytes (Figures S2H–S2L). Overall, TRIM16 attenuates lipid accumulation and inflammation in PAOA-treated hepatocytes.

Hepatocyte-specific TRIM16 deletion exacerbates HFD-induced hepatic steatosis

As lipotoxicity is the leading cause of NAFLD initiation (Schuster et al., 2018), we confirmed the function of TRIM16 in a mouse NAFLD model based on 24 weeks of HFD feeding. Hepatocyte-specific *Trim16* knockout (*Trim16*-HKO) mice were generated (Figures S3A and S3B). Western blot and qPCR analyses confirmed the suppression of TRIM16 expression in the livers of *Trim16*-HKO mice (Figures S3C and S3D). *Trim16*-HKO mice that were fed a normal diet, negative control (NC), showed no difference in body weight, liver weight, insulin resistance (IR), or lipid content compared with *Trim16*-Flox mice (Figures S3E–S3J). However, *Trim16*-HKO mice that were fed an HFD for 24 weeks exhibited higher liver weights and liver weight-to-body weight ratios than the control mice (Figures 2A and S3F). *Trim16*-HKO mice also showed higher fasting blood glucose and more severe insulin resistance (IR), as indicated by glucose tolerance tests (GTTs), and impaired insulin secretion, as indicated by insulin tolerance tests (ITTs) (Figures S3G–S3I). Additionally, hepatic TRIM16 deletion resulted in increased TG/TC levels in the liver and serum (Figures 2B and S3J). Severe lipid accumulation was observed in the livers of HFD-fed *Trim16*-HKO mice (Figure 2C), accompanied by increased expression of genes related to lipid uptake (*Fatp1*), transport (*Fabp1*), and synthesis (*Fasn* and *Acca*) (Figure 2D). However, TRIM16 depletion inhibited the expression of genes participating in lipid β-oxidation (*Pparα* and *Cpt1a*) and utilization (*Pdk4* and *Ucp2*) (Figure 2D). Furthermore, the livers of the *Trim16*-HKO mice were injured to a greater extent in response to HFD feeding, as evidenced by higher alanine aminotransferase (ALT) and aspartate aminotransferase (AST) levels than those of the control group (Figure 2E). These findings reveal that TRIM16 genetic deletion aggravates NAFLD progression.

Trim16-HKO exacerbates HFHC-induced NASH

Given that NASH is the advanced stage of NAFLD (Friedman et al., 2018), we investigated the role of TRIM16 in a mouse NASH model that was induced by 16 weeks of an HFHC diet feeding (Jian et al., 2020). Despite no difference in body weight, *Trim16*-HKO mice that were fed an HFHC diet for 16 weeks

---

(C) Representative hematoxylin and eosin (H&E) (upper) and oil red O (lower) staining of the liver sections of the mice in the indicated group (more than 10 fields of 6 biological replicates for each group). Scale bars, 100 μm.

(D) Relative mRNA levels of genes related to fatty acid metabolism in the livers of the mice in the indicated group (3 technical replicate of 4 biological replicates for each group).

(E) Serum ALT and AST concentrations of the mice in the indicated group (1 technical replicate of 9–10 biological replicates for each group).

(F) Ratios of liver weight to body weight of *Trim16*-HKO and *Trim16*-Flox mice after NC or HFHC consumption for 16 weeks (1 technical replicate of 9–10 biological replicates for each group).

(G) Representative H&E (upper) and oil red O (lower) staining of the liver sections of the mice in the indicated group (more than 10 fields of 6 biological replicates for each group). Scale bars, 100 μm.

(H) Relative mRNA levels of genes related to fatty acid metabolism in the livers of the mice in the indicated group (3 technical replicate of 4 biological replicates for each group).

(I) Representative immunofluorescence staining images of CD11b (red, upper) and F4/80 (red, lower) of the liver sections of the mice in the indicated group (more than 10 fields of 4 biological replicates for each group), in which nuclei were stained with DAPI (blue). Scale bars, 50 μm. The lower panels show quantification of CD11b and F4/80 positive cells in each filed.

(J) Relative mRNA levels of proinflammatory genes in the livers of the mice in the indicated group (3 technical replicate of 4 biological replicates for each group).

(K) Representative PSR (upper) and Masson (lower) staining of the liver sections of the mice in the indicated group (more than 10 fields of 6 biological replicates for each group). Scale bars, 100 μm.

(L) Relative mRNA levels of profibrotic genes in the livers of the mice in the indicated group (3 technical replicate of 4 biological replicates for each group).

(M) Serum ALT and AST concentrations in the mice in the indicated group (1 technical replicate of 10 biological replicates for each group).

In all statistical plots, data are expressed as the mean ± SD. For (A), (B), (E), (F), and (M), statistical analyses were carried out by one-way ANOVA with Bonferroni post hoc analysis for data meeting homogeneity of variance requirements or Tamhane's T2(M) post hoc analysis for heteroscedastic data. For (D), (H)–(J), and (L), statistical analyses were carried out by two-tailed Student's t test. Gene expressions were normalized to ACTB. *p < 0.05, **p < 0.01, *Trim16*-HKO HFD group versus *Trim16*-Flox HFD group, or *Trim16*-HKO HFHC group versus *Trim16*-Flox HFHC group; ALT, alanine aminotransferase; AST, aspartate aminotransferase. See also Figures S3–S5 and Tables S3, S4, and S7.

Cell Metabolism
Article

CellPress
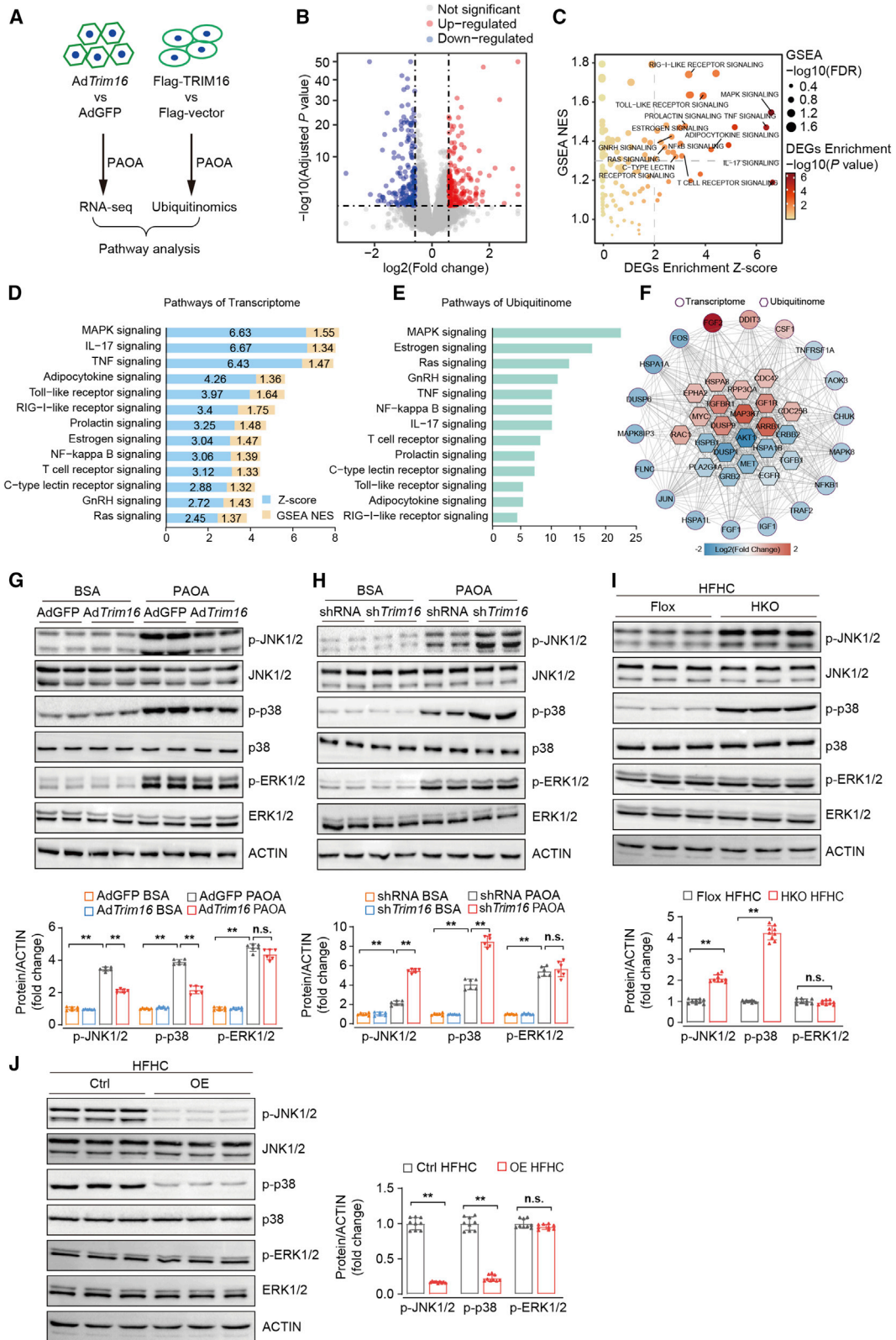
displayed greater liver weights, greater liver weight-to-body weight ratios, higher fasting blood glucose, and more severe IR than *Trim16*-Flox mice (Figures 2F and S4A–S4D). The TG/TC concentration in the livers and serum of the *Trim16*-HKO mice also increased in the context of NASH (Figures S4E and S4F). Hematoxylin and eosin (H&E) and oil red O staining demonstrated that hepatic steatosis was more severe in the *Trim16*-HKO mice compare with the control mice (Figure 2G). Consistently, the *Trim16*-HKO mice exhibited higher mRNA levels of genes related to fatty acid uptake and synthesis (Figure 2H).

Next, indicators of inflammation and fibrosis in NASH were examined (Hwang et al., 2020; Liu et al., 2020). We found intensified infiltration of inflammatory cells and enhanced proinflammatory gene expression in HFHC-fed *Trim16*-HKO mice compare with *Trim16*-Flox mice (Figures 2I, 2J, and S4G). Furthermore, *Trim16*-HKO resulted in fibrosis, as indicated by picrosirius red (PSR) and Masson staining, and the upregulated expression of profibrotic genes in liver (Figures 2K and 2L). Similarly, hepatic TRIM16 deficiency potentiated the serum levels of ALT and AST (Figure 2M).

Next, we separated out the liver tissues of HFHC-fed *Trim16*-HKO and control mice and performed RNA-seq, followed by hierarchical clustering analysis, to systematically depict the gene expression profile of TRIM16 deletion in the context of NASH (Figure S4H). We found that hepatic TRIM16 deficiency caused extensive upregulation of pathways and genes promoting lipogenesis, inflammation, fibrosis, and apoptosis in the context of NASH (Figures S4I and S4J). In summary, TRIM16 depletion intensifies NASH in mice.

Hepatocyte-specific TRIM16 overexpression ameliorates HFHC-induced NASH

To further verify the function of hepatic TRIM16 in NASH pathogenesis, we generated hepatocyte-specific TRIM16 overexpression (OE) mice by delivering liver-specific pT3 plasmid carrying *Trim16* and the SB100X transposase plasmids into the mice (Kodama et al., 2018; Moon et al., 2019). Western blot and qPCR analyses confirmed the hepatocyte-specific overexpression of TRIM16 (Figures S5A and S5B). The OE mice exhibited lower liver weights and liver weight-to-body weight ratios, but not lower body weights, than the control mice after 16 weeks of HFHC feeding (Figures S5C and S5D). HFHC-induced higher

blood glucose and more severe IR were ameliorated by TRIM16 overexpression (Figures S5E and S5F). Furthermore, the OE mice displayed a lower degree of hepatic steatosis than their counterparts (Figures S5G–S5J). Also, TRIM16 overexpression substantially mitigated inflammation, fibrosis, and liver injury during NASH progression (Figures S5K–S5N). Overall, TRIM16 overexpression inhibits NASH progression.

TRIM16 suppresses the JNK-p38 signaling pathway in NASH

Given that TRIM16 is an E3 ligase, conjoint analysis of transcriptomics and ubiquitinomics was performed to explore the underlying pathway accounting for the cytoprotective function of TRIM16 in response to lipotoxicity (Figure 3A). Kyoto Encyclopedia of Genes and Genomes (KEGG) analysis and GSEA of the transcriptomics presented 13 pathways significantly regulated by TRIM16 overexpression, among which the MAPK signaling pathway possessed the highest enrichment score (Figures 3B–3D). Consistently, the ubiquitinomics analysis revealed that TRIM16 predominantly linked ubiquitin to molecules in the MAPK signaling pathway (Figure 3E). The joint analysis showed that TRIM16 had extensive impact on the MAPK family members (Figure 3F). Taken together, these bioinformatic results identify the MAPK pathway as the candidate signaling pathway regulated by TRIM16 in NASH pathogenesis.

Next, we confirmed by western blot analyses that the activation of JNK1/2 and p38 was inhibited by TRIM16 overexpression but enhanced by TRIM16 deletion in PAOA-treated hepatocytes. However, ERK1/2 phosphorylation was not affected by TRIM16 overexpression or deletion (Figures 3G and 3H). The results were further verified by *in vivo* assays (Figures 3I and 3J). Overall, TRIM16 inhibits the activation of the JNK-p38 pathway in the context of NASH.

TRIM16 interacts with TAK1 and promotes K48-linked ubiquitination

To identify the specific target mediating the suppression of the JNK-p38 pathway by TRIM16, we carried out immunoprecipitation-mass spectrometry (IP-MS) analysis using TRIM16-overexpressing L02 hepatocytes and then integrated the results of IP-MS and quantitative ubiquitinomics (Figure 4A). Six candidate MAPK members were identified in the interactome analysis, and

---

Figure 3. TRIM16 suppresses the JNK-p38 signaling pathway in NASH

(A) Scheme showing the procedure of identifying the signaling pathways regulated by TRIM16 in the setting of lipotoxicity.

(B) A volcano plot showing DEGs (red, upregulated genes; blue, downregulated genes) in mouse primary hepatocytes infected with Ad*Trim16* or AdGFP treated with PAOA.

(C) GSEA combined with KEGG analysis of the data of RNA-seq.

(D) Histogram summarizing the GSEA NES and *Z* score of the 13 pathways presented in (C).

(E) Ubiquitinomics analysis assessing the 13 pathways presented in (D) according to the ubiquitination occurring in them.

(F) Intersection analysis showing the MAPK family members detected by the transcriptome in and ubiquitinomics.

(G and H) Representative western blot images showing phosphorylated and total protein levels of TAK1, JNK, p38, and ERK in primary hepatocytes infected with Ad*Trim16* or AdGFP (G) and Adsh*Trim16* or AdshRNA (H) with PAOA or BSA treatment. Western blot images are followed by semi-quantitative analyses (1 technical replicate of 6 biological replicates for each group).

(I and J) Representative western blot images showing phosphorylated and total protein levels of TAK1, JNK, p38, and ERK in the livers of HFHC-fed *Trim16*-HKO and *Trim16*-Flox mice (I) or *Trim16*-OE mice and their controls (J). Western blot images are followed by semi-quantitative analyses (1 technical replicate of 9–10 biological replicates for each group).

In all statistical plots, data are expressed as the mean ± SD. For (G) and (H), statistical analyses were carried out by one-way ANOVA with Bonferroni post hoc analysis for data meeting homogeneity of variance requirements or Tamhane's T2(M) post hoc analysis for heteroscedastic data. For (I) and (J), statistical analyses were carried out by two-tailed Student's t test, *p < 0.05, **p < 0.01; n.s., not significant. See also Table S3.
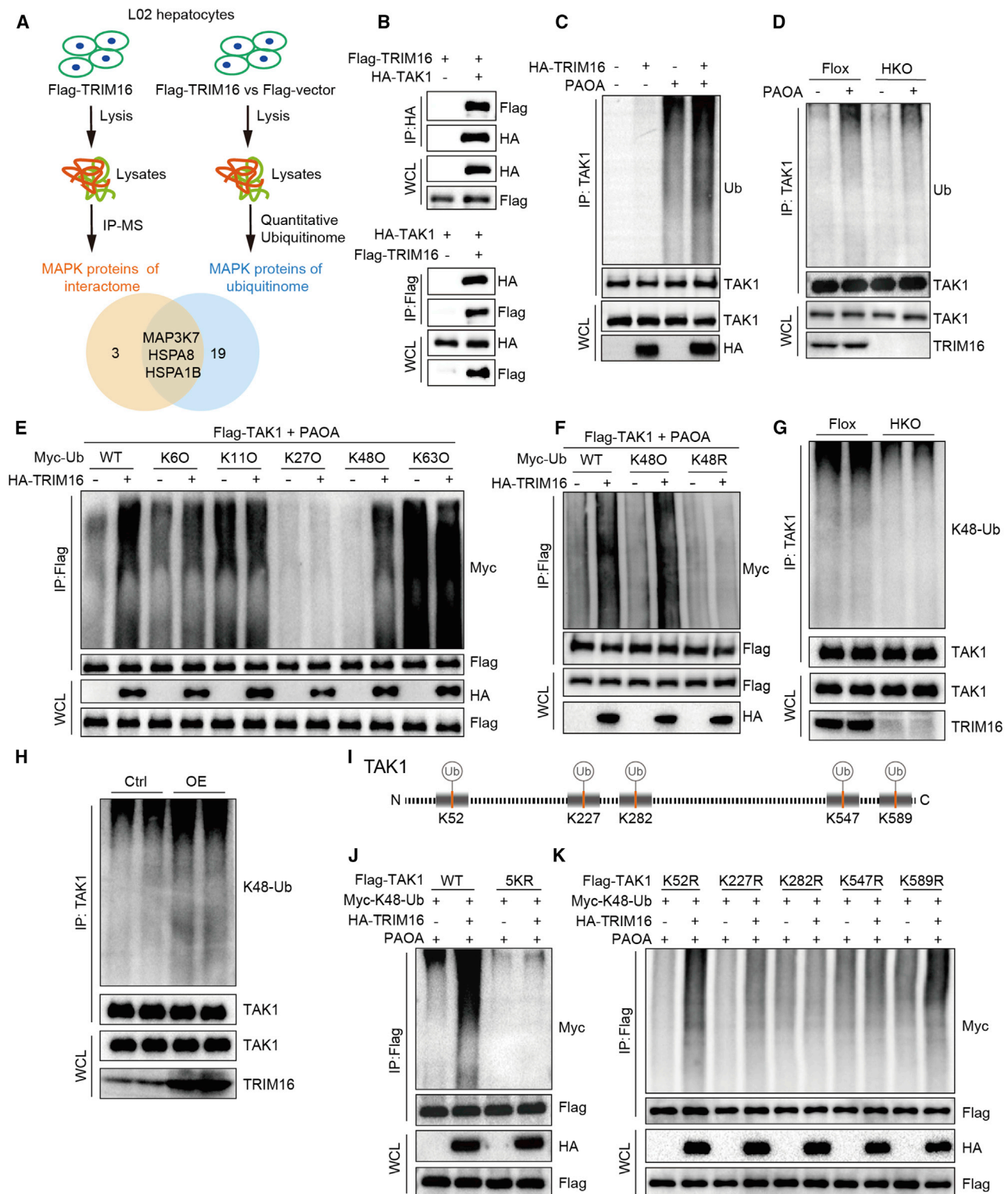
Figure 4. TRIM16 interacts with TAK1 and promotes K48-linked ubiquitination

(A) Scheme showing the procedure of identifying the downstream targets of TRIM16 by the intersection analysis of IP-MS and quantitative ubiquitinomics.

(B) Coimmunoprecipitation (coIP) assays were performed to examine the interaction of TRIM16 and TAK1 in 293T cells transfected with the indicated plasmids. WCL, whole-cell lysis.

(C) Ubiquitination assays determining the ubiquitination of endogenous TAK1 in L02 hepatocytes transfected with HA-TRIM16 or negative control plasmids, with or without PAOA treatment.

(legend continued on next page)

Cell Metabolism
Article

CellPress

three of them (MAPK37, HSPA8, and HSPA1B) were also present in the ubiquitination proteomic results that contained 22 candidates (Figure 4A). Numerous studies have proved the pivotal regulatory function of TAK1 (MAP3K7) in NASH progression (Ji et al., 2018; Liu et al., 2020). Accordingly, TAK1 was selected as the candidate target of TRIM16. To confirm the results of the interactome, immunofluorescence staining was performed in L02 hepatocytes, and a specific interaction between TRIM16 and TAK1 was observed by confocal microscopy (Figure S6A). This result was supported by reciprocal coimmunoprecipitation (coIP) analysis (Figure 4B). Furthermore, the glutathione S-transferase (GST) precipitation assay revealed a direct interaction between TRIM16 and TAK1 (Figure S6B). Subsequently, molecular mapping assays revealed that the C terminus (SPRY/B30.2 domain) of TRIM16 was responsible for its direct interaction with the N-terminal kinase domain of TAK1 (Figures S6C and S6D).

To verify the results of ubiquitinomics, we performed protein ubiquitination assays and found that TRIM16 facilitated the ubiquitination of both endogenous and exogenous TAK1 in PAOA-treated hepatocytes (Figures 4C and S6E). In contrast, hepatocytes isolated from *Trim16*-HKO mice, and thus deficient for Trmp16 expression, were hampered in the ubiquitination of TAK1 (Figure 4D). Screening of mutated forms of ubiquitin for potential lysine ubiquitination types revealed that in the setting of PAOA treatment, both wild-type (WT) Ub and K48O (Ub with the intact Lys48 residue alone) could be linked to TAK1 by TRIM16, but not K6O, K11O, K27O, or K63O (Figure 4E). Moreover, TRIM16 failed to link K48R (Ub only Lys48 residue was mutated) to TAK1 (Figure 4F), indicating that TRIM16 predominantly promoted K48-linked ubiquitination on TAK1. We observed that TAK1 K48-linked ubiquitination was decreased in the livers of HFHC-fed *Trim16*-HKO mice (Figure 4G) and increased in that of TRIM16-overexpressing mice (Figure 4H). To determine potential TRIM16-catalyzed lysine sites, the five lysine sites of TAK1 was mutated in combination (TAK1-5KR) or separately (TAK1-K52R/K227R/K282R/K547R/K589R), according to the predicted results of ubiquitinomics (Figure 4I). We found that TRIM16 could not promote K48-linked ubiquitination on TAK1-5KR (Figure 4J), whereas mutation of K282 and K547 abolished TRIM16-mediated ubiquitination, indicating that K282 and K547 sites were the specific sites responsible for TRIM16-catalyzed ubiquitination of TAK1 under PAOA treatment (Figure 4K).

TRIM16 facilitates the proteasomal degradation of phospho-TAK1

Next, we investigated the impact of TRIM16-catalyzed ubiquitination on TAK1. We found by western blot analyses that TAK1 phosphorylation was attenuated in TRIM16-overexpressing he-

patocytes, but intensified in TRIM16- downregulated hepatocytes treated with PAOA. However, it was surprising that the level of total TAK1 remained unchanged (Figures 5A and 5B), as it has been reported that K48-linked polyubiquitination predominantly targets TAK1 for proteasomal degradation (Ahmed et al., 2011). The results indicated that TRIM16 might predominantly promote the proteasomal degradation of p-TAK1 instead of the total TAK1. As expected, TRIM16 lost the inhibitory effect on p-TAK1 when we used MG132, a proteasome inhibitor, in the assay (Figure 5C).

Next, we tested the interaction between p-TAK1 and TRIM16. We found that the interaction was strengthened in PAOA-treated hepatocytes, which occurred in parallel with an increase of p-TAK1 (Figure 5D). Furthermore, we utilized lambda protein phosphatase (λ-PPase), which catalyzes the dephosphorylation of phosphorylated proteins, and found that λ-PPase markedly reduced the interaction between p-TAK1 and TRIM16 (Figure 5E). Consistent with these results, the interaction could also be notably inhibited by 5Z-7-Oxozeaenol (5Z-7) (Figure 5F), which selectively attenuates the phosphorylation of TAK1 (Ninomiya-Tsuji et al., 2003).

These findings suggest that TRIM16 might physically interact with p-TAK1. To further test this possibility, we constructed TAK1-4A and -4D, in which four phosphorylation sites (T184, T187, S192, and S412) were substituted by alanine or aspartic acid, respectively. TAK1-4A, which could not be phosphorylated or activated, showed a slight interaction with TRIM16 (Figure 5G). In contrast, TAK1-4D, the constitutively activated mutation, showed an intensified interaction with TRIM16 (Figure 5H). Overall, these data show that TRIM16 preferentially interacts with p-TAK1 in response to lipotoxicity.

Subsequently, we sought to determine whether TRIM16 could facilitate K48-linked ubiquitination of p-TAK1. We found that 5Z-7 abolished TRIM16-catalyzed K48-linked ubiquitination of both endogenous and exogenous TAK1 in PAOA-treated hepatocytes (Figures 5I and 5J). Consistent with these results, we also found that TRIM16 linked K48-Ub to both TAK1 and the TAK1-4D mutant but not to the TAK1-4A mutant (Figure 5K), indicating that TRIM16 predominantly catalyzes K48-linked ubiquitination of p-TAK1. Overall, TRIM16 preferentially interacts with p-TAK1 and promotes its proteasomal degradation by catalyzing K48-linked ubiquitination at the K282 and K547 sites in the context of lipotoxicity.

Inhibition of TAK1 abolishes the enhanced NASH progression caused by TRIM16 deficiency

Next, we validated the TRIM16-TAK1 regulatory axis in NASH progression. We found that 5Z-7 suppressed the activated TAK1-JNK-p38 signaling pathway resulting from TRIM16

(D) Ubiquitination assays determining the ubiquitination of endogenous TAK1 in primary hepatocytes isolated from *Trim16*-HKO or *Trim16*-Flox mice, and then treated with PAOA or BSA.

(E and F) In screening for potential lysine ubiquitination types, the ubiquitination of Flag-TAK1 in response to TRIM16 overexpression was examined in L02 hepatocytes transfected with the wild-type (WT) and mutated Myc-Ub plasmids and treated with PAOA.

(G and H) Ubiquitination assays determining the ubiquitination of endogenous TAK1 in the livers of *Trim16*-HKO (G), *Trim16*-OE (H), and their corresponding control mice with HFHC administration.

(I) Sketch map showing the TRIM16-catalyzed ubiquitinated sites on TAK1 predicted by the ubiquitinomics.

(J and K) Ubiquitination assays determining the ubiquitination of TAK1-5KR or TAK1-K52R/K227R/K282R/K547R/K589R in response to TRIM16 overexpression in L02 hepatocytes transfected with the indicated plasmids and treated with PAOA. All experiments above have 1 technical replicate of 3 biological replicates for each group. See also Figure S6 and Table S5.
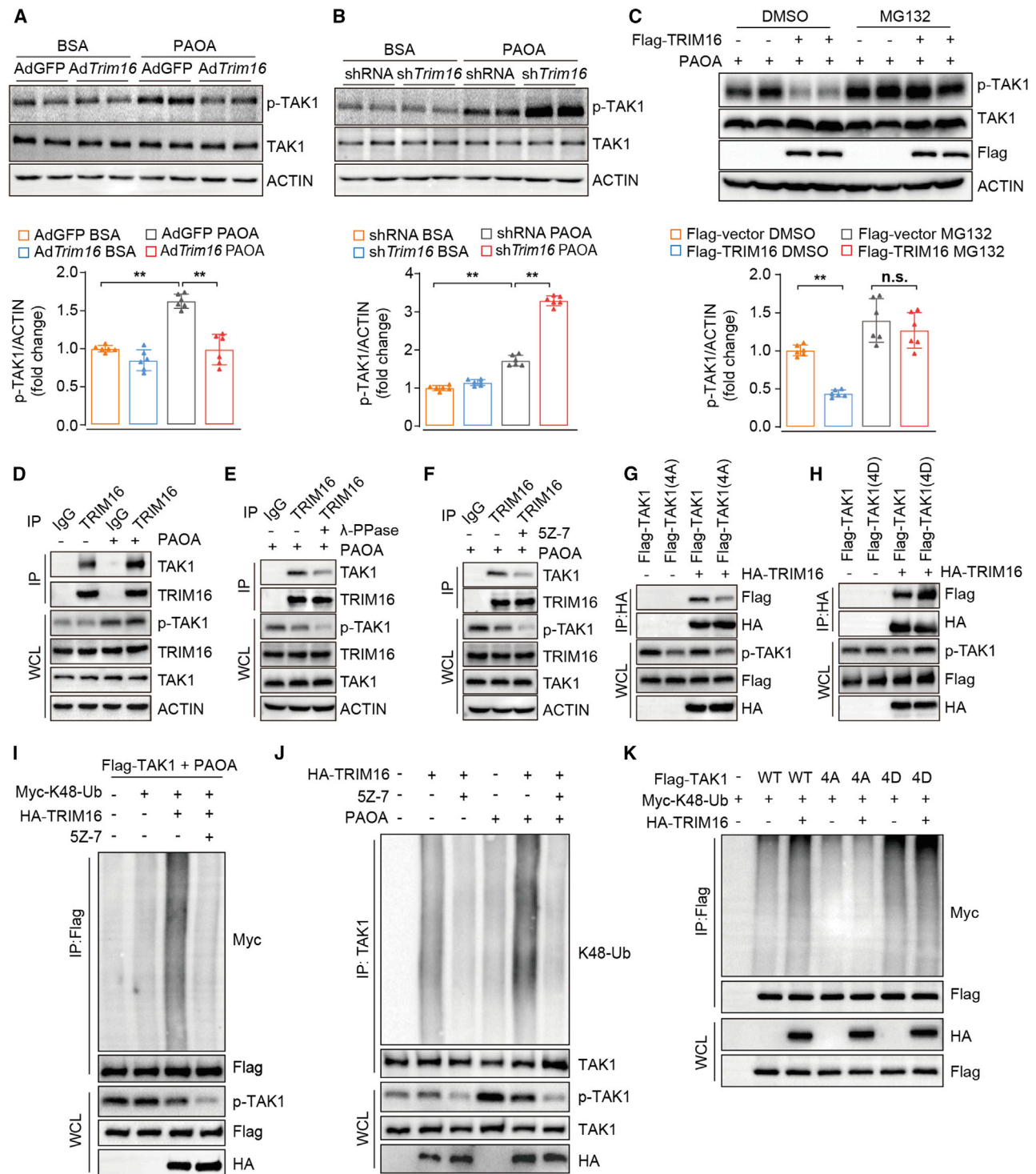
Figure 5. TRIM16 facilitates the proteasomal degradation of phospho-TAK1

(A and B) Representative western blot image showing the expression of the indicated proteins in mouse primary hepatocytes infected with AdGFP and Ad*Trim16* (A) or AdshRNA and Adsh*Trim16* (B), with PAOA or BSA treatment. The lower panels show semi-quantitative analyses of the western blot results (1 technical replicate of 6 biological replicates for each group).

(C) Representative western blot image showing the level of p-TAK1 and TAK1 in L02 hepatocytes transfected with HA-TRIM16 plasmid and treated with or without MG132. The lower panels show semi-quantitative analyses of the western blot results (1 technical replicate of 6 biological replicates for each group).

(D) CoIP assay showing the interaction of endogenous TRIM16 and TAK1 in mouse primary hepatocytes with or without PAOA stimulation.

deletion in PAOA-treated primary hepatocytes of *Trim16*-HKO mice (Figure S7A). Moreover, 5Z-7 mitigated the enhanced fatty acid synthesis and proinflammatory gene expression (Figures S7B–S7D). In parallel with the results of *in vitro* experiments, 5Z-7 administration significantly attenuated aberrant activation of TAK1 cascades in the liver of *Trim16*-HKO mice after HFHC treatment for 16 weeks (Figure 6A). Furthermore, the phenotypic and transcriptional alterations induced by HFHC administration in *Trim16*-HKO mice could be ameliorated by the use of 5Z-7 (Figures 6B–6J). These findings further verify that TRIM16 exert its cytoprotective function in NASH by regulating TAK1.

TRIM16 overexpression by adeno-associated virus attenuates hepatic steatosis and inflammation in HFHC-fed mice

Finally, we examined the therapeutic efficacy of TRIM16 in NASH. We injected adeno-associated virus 8 (AAV8) expressing TRIM16 (AAV-*Trim16*) into 8-week-old HFHC-fed mice and continued to feed them with an HFHC diet for another 8 weeks. Western blot and qPCR analyses confirmed the overexpression of TRIM16 in the livers of AAV-*Trim16*-injected mice (Figures 7A and 7B). Compared to the control group (AAV-GFP), the AAV-*Trim16*-injected mice showed significantly decreased liver weights and liver-weight-to-body-weight ratios after 16 weeks of HFHC consumption, with marginal changes in body weight (Figure 7C). In addition, the AAV-mediated overexpression of TRIM16 substantially moderated lipid accumulation, inflammation, fibrosis, and liver injury in the livers of HFHC-fed mice (Figures 7D–7K).

DISCUSSION

Lipotoxicity is a major trigger of hepatocyte dysfunction and hepatotoxicity in the context of NASH (Ibrahim et al., 2018; Song and Malhi, 2019). Excessive lipids, especially the saturated fatty acids palmitate (C16:0), stearate (C18:0), and cholesterol, can induce aberrant activation of kinases and downstream JNK, as well as mitochondrial-death-related pathways (Brenner et al., 2013; Da Silva Morais et al., 2009; Schuster et al., 2018). To identify crucial ubiquitin-related molecules that can restrict the hyperactivation of kinases, we conduct integrative multiomics analysis, finding the upregulation of TRIM16 in response to lipotoxicity.

TRIM16 has been documented as a cytoprotective molecule by exerting E3 ligase activity. A previous study has shown that TRIM16, together with Galectin-3, protects cells from lysosomal damage by activating selective autophagy (Chauhan et al., 2016). Under proteotoxic stress caused by protein aggregates,

TRIM16 acts on the p62-NRF2 axis, leading to ubiquitination of misfolded proteins (Jena et al., 2018). Moreover, TRIM16 confers a cytoprotective effect in oxygen-glucose deprivation/reoxygenation-exposed neurons, by enhancing the Nrf2-ARE antioxidant signaling pathway (Ren et al., 2020). In this study, we also show that TRIM16 can protect hepatocytes from lipotoxicity in NASH models by catalyzing ubiquitination-dependent degradation of p-TAK1. Notably, TRIM16's cytoprotective function is further validated in an AAV8-mediated therapeutic model *in vivo* in mice. Given that AAV-mediated gene replacement, gene silencing, and gene editing have exhibited a great deal of success in preclinical and clinical situations (Wang et al., 2019), AAV-mediated TRIM16 overexpression promises to be an effective treatment to mitigate hepatic steatosis and inflammation in NASH.

TAK1 has been identified as a crucial regulatory component of MAPK and nuclear factor-κB (NF-κB) signaling pathways (Ajibade et al., 2013), both of which play a key role in lipid metabolism and inflammation (Lawan and Bennett, 2017; Michelotti et al., 2013). Accordingly, TAK1 confers pivotal regulatory functions in NASH pathogenesis including autophagy, inflammation, and hepatic steatosis (Cai et al., 2018; Inokuchi-Shimizu et al., 2014; Wu et al., 2020b). In response to proinflammatory stimulation, the E3 ligase TRAF2 or TRAF6 catalyzes K63-linked polyubiquitination of TAK1, and then TAK1 autophosphorylates at the T184/187 and S192 sites to achieve full activation. Activated TAK1 then phosphorylates downstream substrates to spark the NF-κB and MAPK signaling pathways (Ajibade et al., 2013). Hence, phospho-TAK1 confers most of its regulatory functions, and inhibiting the hyperactivation of TAK1 should be a promising NASH therapy. In the present study, we validated the ubiquitination-mediated degradation of p-TAK1 by TRIM16.

Phosphorylation-dependent ubiquitination has been investigated in several studies. A well-elucidated mechanism is the precise regulation of Skp1/cullin/F box protein (SCF) ubiquitin ligases to their phosphorylated substrates (Winston et al., 1999). Additionally, Hiroaki Nagai et al. report that oxidative stress-induced ASK1 phosphorylation is a prerequisite for USP9X-mediated ubiquitination (Nagai et al., 2009). Here, we also demonstrate that TRIM16 catalyzed K48-linked ubiquitination of p-TAK1. However, unlike SCF- or USP9X-mediated ubiquitination, which exclusively acts on phosphorylated substrates, TRIM16-mediated ubiquitination takes place on both TAK1 and p-TAK1, as our results show that the 4A mutation of TAK1 could not completely remove its interaction with TRIM16. Consistent with our findings, Neesar Ahmed's group also showed that the Itch-Cyld complex sequentially cleaves K63-linked ubiquitin chains and catalyzes K48-linked ubiquitination of not only


(E and F) CoIP assays showing the interaction between TAK1 and TRIM16 in PAOA-treated L02 hepatocytes transfected with the indicated plasmids with or without lambda protein phosphatase (λ-PPase) (E) or 5Z-7-Oxozeaenol (5Z-7) (F) treatment.

(G and H) CoIP assays showing the interaction of TRIM16 and TAK1-4A mutation (G) or TAK1-4D mutation (H) in L02 hepatocytes transfected with the indicated plasmids.

(I and J) Ubiquitination assays determining the ubiquitination of ectogenic TAK1 (I) or endogenous TAK1 (J) in L02 hepatocytes transfected with the indicated plasmids and treated with PAOA or 5Z-7 as indicated.

(K) Ubiquitination assays determining the ubiquitination of WT and 4A/4D mutated TAK1 in response to TRIM16 overexpression in L02 hepatocytes transfected with the indicated plasmids and treated with or without PAOA.

In all statistical plots, data are expressed as the mean ± SD. All statistical analyses were carried out by one-way ANOVA with Bonferroni post hoc analysis for data meeting homogeneity of variance requirements or Tamhane's T2(M) post hoc analysis for heteroscedastic data. **p < 0.01; n.s., not significant. In (D)–(K), 1 technical replicate of 3 biological replicates for each group. See also Table S5.

Cell Metabolism
Article

CellPress
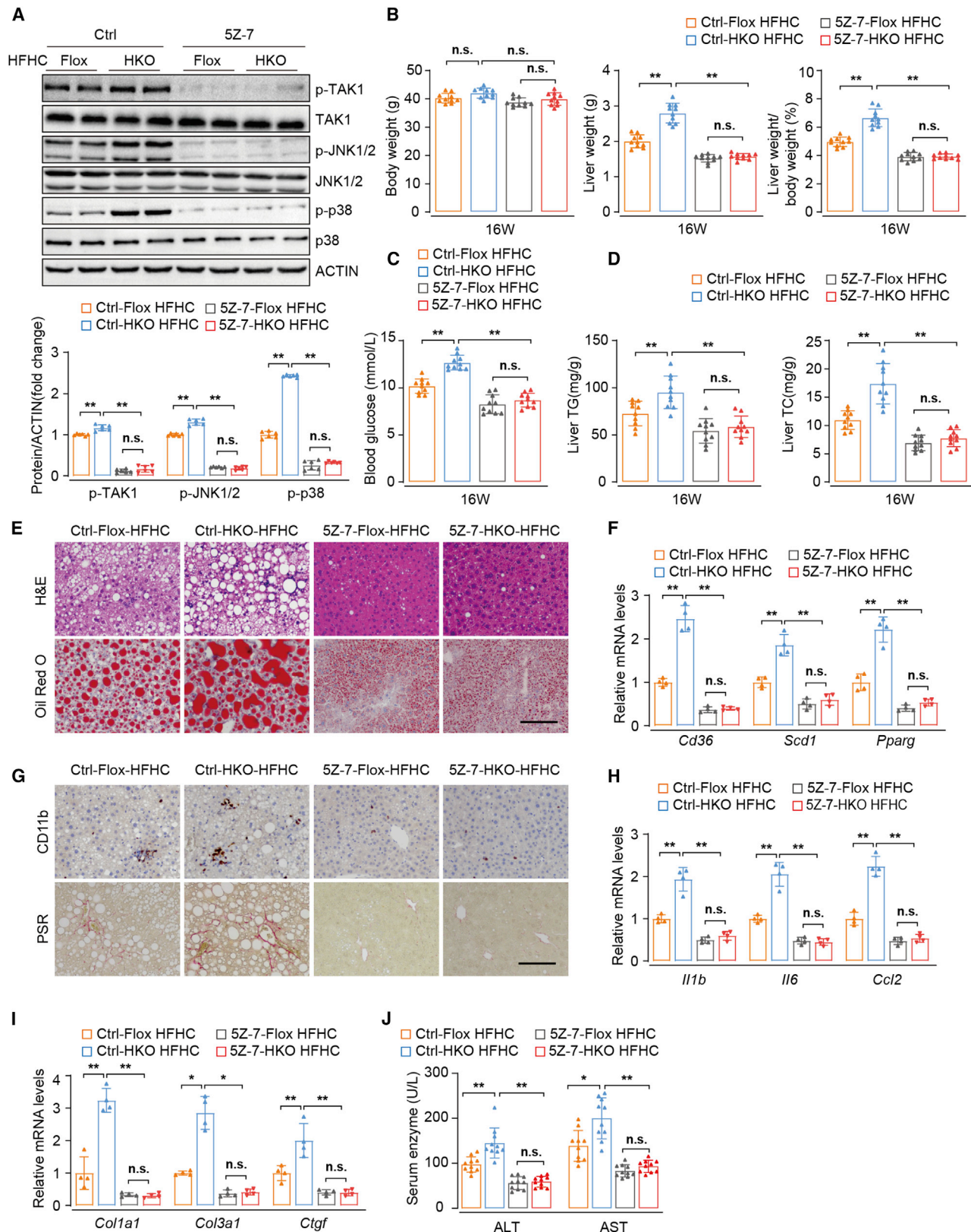
TAK1 but also p-TAK1 (Ahmed et al., 2011). One explanation for the discrepancy may be that phosphorylation itself could create a binding site for an E3 ligase (Hunter, 2007; Wu et al., 2003). However, TAK1 might not be subjected to such kinase activity-dependent conformational changes.

Although the crosstalk between ubiquitination and phosphorylation on TAK1 and ASK1 is noteworthy, none of the studies mentioned above have elucidate the underlying mechanism. Nevertheless, we speculate that ubiquitination regulation of phosphorylation might be a precise way to maintain the homeostasis of crucial activated kinases. Both ASK1 and TAK1 play a critical role in the initiation and progression of the MAPK signaling pathway (Mihaly et al., 2014; Takeda et al., 2008). Due to the importance of the MAPK pathway in regulating many physiological and pathological processes, either excessive activation or total depletion of TAK1 leads to disrupted signaling cascades, resulting in cell injury or death (Inokuchi-Shimizu et al., 2014; Yang et al., 2013). Hence, the phosphorylation-dependent ubiquitination of TAK1 might be a refined regulatory mechanism to degrade only the small part of hyperactivated TAK1 in the context of NASH, without affecting other p-TAK1-mediated biological processes needed for homeostasis. This hypothesis is supported by our results. Namely, TRIM16 overexpression or depletion has no effect on phenotypic changes in BSA-treated hepatocytes or normal-diet-fed mice; TRIM16 overexpression attenuates TAK1 phosphorylation in PAOA-treated hepatocytes, but not BSA-treated hepatocytes; and PAOA treatment enhances the interaction between TRIM16 and TAK1, as well as the TAK1 ubiquitination catalyzed by TRIM16. Although in-depth investigation of this hypothesis is needed, our study suggests a refined regulation of p-TAK1 by TRIM16. Consequently, targeting TRIM16 might be an effective treatment for NASH that can avoid potential unwanted side effects.

In conclusion, this study reveals that TRIM16 facilitates ubiquitination-mediated degradation of p-TAK1, which subsequently inhibits the activated JNK-p38 cascades in NASH progression. Our study identifies TRIM16 as a precise suppressor of activated TAK1 and a promising therapeutic target for the treatment of NASH in the clinic.

Limitations of study

This study indicates that TRIM16 preferentially interacts with PAOA-induced p-TAK1. However, a specific mechanism deserves to be further investigated. This study reveals that TRIM16 controls hepatic lipid accumulation and inflammation through the regulation of p-TAK1; however further research is needed for a more detailed explanation of this process. Further, the correlation between TRIM16 and NASH remains to be tested in large-scale clinical studies, including correlating reduced TRIM16 expression with disease severity among patients with NASH. And lastly, the targeting of TRIM16 in large animal models of NASH, such as nonhuman primates, is needed before proceeding to its testing in the clinic.

STAR★METHODS

Detailed methods are provided in the online version of this paper and include the following:

- KEY RESOURCES TABLE
- RESOURCE AVAILABILITY
  - Lead Contact
  - Materials availability
  - Data and code availability
- EXPERIMENTAL MODEL AND SUBJECT DETAILS
  - Mice
  - Primary hepatocytes
  - Cell lines
  - Human liver samples
- METHOD DETAILS
  - Generation of genetically modified mice
  - Mouse metabolic and liver function assays
  - Lipid analysis
  - Histopathological analysis
  - Immunofluorescence staining and confocal microscopy
  - Cellular Nile Red staining
  - LDH analysis
  - Dual-luciferase reporter assay
  - Plasmid construction and viral infection

Figure 6. Inhibition of TAK1 abolishes the enhanced NASH progress caused by TRIM16 deficiency

(A) Representative western blot images showing phosphorylated and total protein levels of TAK1, JNK, and p38 in the livers of HCFC-fed *Trim16*-HKO and *Trim16*-Flox mice with or without 5Z-7 administration. The lower panel shows semi-quantitative analysis of the western blotting results (1 technical replicate of 6 biological replicates for each group).

(B–D) Body weights, liver weights, ratios of liver weight to body weight (B), fasting blood glucose levels (C), and hepatic TG and TC contents (D) of the mice in the indicated groups (1 technical replicate of 10 biological replicates for each group).

(E) Representative H&E and oil red O staining of the liver sections of the mice in the indicated groups (more than 10 fields of 6 biological replicates for each group). Scale bars, 100 μm.

(F) Relative mRNA levels of fatty acid metabolism related genes in liver of the mice in the indicated groups (3 technical replicate of 4 biological replicates for each group).

(G) Representative immunohistochemistry staining of CD11b and PSR staining of liver sections of the mice in the indicated groups (more than 10 fields of 6 biological replicates for each group). Scale bars, 100 μm.

(H and I) Relative mRNA levels of proinflammatory genes (H) and profibrotic genes (I) in livers of the mice in the indicated groups (3 technical replicate of 4 biological replicates for each group).

(J) Serum ALT and AST levels of the mice in the indicated groups (1 technical replicate of 10 biological replicates for each group).

In all statistical plots, data are expressed as the mean ± SD. All statistical analyses were carried out by one-way ANOVA with Bonferroni post hoc analysis for data meeting homogeneity of variance requirements or Tamhane's T2(M) post hoc analysis for heteroscedastic data. For (A), (F), (H), and (I), gene expressions were normalized to ACTB. $*p < 0.05$, $**p < 0.01$; n.s., not significant; ALT, alanine aminotransferase, AST, aspartate aminotransferase. See also Figure S7 and Table S7.
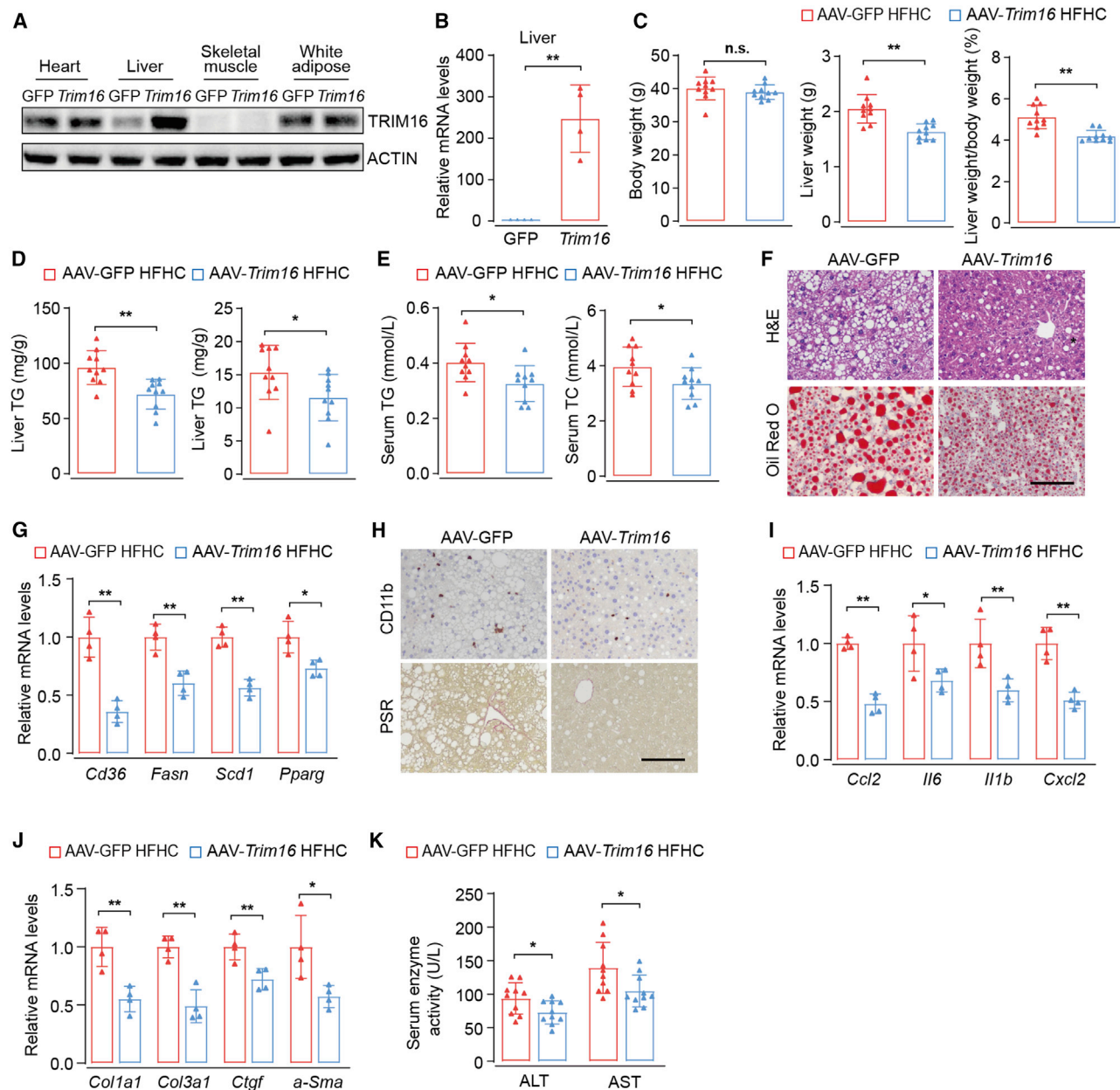
Figure 7. TRIM16 overexpression by adeno-associated virus attenuates hepatic steatosis and inflammation in HFHC-fed mice

(A) Representative western blot image showing TRIM16 protein level in the organs of HFHC-fed mice injected with AAV-GFP or AAV-*Trim16* (1 technical replicate of 2 biological replicates for each group).

(B) Relative mRNA levels of TRIM16 in livers of the mice in the indicated groups (3 technical replicate of 4 biological replicates for each group).

(C) Body weights, liver weights, and ratios of liver weight to body weight of the mice in the indicated groups (1 technical replicate of 10 biological replicates for each group).

(D and E) TG and TC contents in the livers (D) and serum (E) of the mice in the indicated groups (3 technical replicate of 10 biological replicates for each group).

(F) Representative H&E and oil red O staining of the liver sections of the mice in the indicated groups (more than 10 fields of 6 biological replicates for each group). Scale bars, 100 μm.

(G) Relative mRNA levels of fatty acid metabolism related genes in liver of the mice in the indicated groups (3 technical replicate of 4 biological replicates for each group).

(H) Representative immunohistochemistry staining of CD11b and PSR staining of liver sections of the mice in the indicated groups (more than 10 fields of 6 biological replicates for each group). Scale bars, 100 μm.

(I and J) Relative mRNA levels of proinflammatory genes (I) and profibrotic genes (J) in livers of the mice in the indicated groups (3 technical replicate of 4 biological replicates for each group).

(K) Serum ALT and AST levels of the mice in the indicated groups (1 technical replicate of 10 biological replicates for each group).

In all statistical plots, data are expressed as the mean ± SD. All statistical analyses were carried out by two-tailed Student's t test. For (B), (G), (I), and (J), gene expressions were normalized to ACTB. *$p < 0.05$, **$p < 0.01$; n.s., not significant; ALT, alanine aminotransferase; AST, aspartate aminotransferase. See also Table S7.

Cell Metabolism
Article

- ○ Quantitative PCR analysis
- ○ Western blot analysis
- ○ Immunoprecipitation assays
- ○ Ubiquitination assays
- ○ Chromatin Immunoprecipitation (ChIP)
- ○ RNA-seq and data processing
- ○ Identification of candidate genes
- ○ Scanning of TRIM16 promoter-binding transcription factors
- ○ Hierarchical clustering analysis
- ○ Gene set enrichment analysis (GSEA)
- ○ KEGG pathway enrichment analysis
- ○ Mass spectrometry analysis
- ○ Ubiquitinated proteome analysis
- ● QUANTIFICATION AND STATISTICAL ANALYSIS

SUPPLEMENTAL INFORMATION

Supplemental information can be found online at https://doi.org/10.1016/j.cmet.2021.05.019.

AUTHOR CONTRIBUTIONS

L.W. and K.D. designed the experiments. L.W., X.Z., Z.-B.L., and P.Y. performed the experiments and data analysis. Z.-B.L. and P.Y. wrote the manuscript. H.X., J.D., B.R., P.S., J.L., Z.Y., Z.F., H. Hu, Z.L., X.-L.H., L.Y., and S.T. provided technical support. K.T. and H. Han provided advice and comments. L.W. and K.D. organized and supervised the study.

DECLARATION OF INTERESTS

The authors declare no competing interests.

REFERENCES

Ahmed, N., Zeng, M., Sinha, I., Polin, L., Wei, W.Z., Rathinam, C., Flavell, R., Massoumi, R., and Venuprasad, K. (2011). The E3 ligase Itch and deubiquitinase Cyld act together to regulate Tak1 and inflammation. Nat. Immunol. 12, 1176–1183.

Ajibade, A.A., Wang, H.Y., and Wang, R.F. (2013). Cell type-specific function of TAK1 in innate immune signaling. Trends Immunol. 34, 307–316.

Arab, J.P., Arrese, M., and Trauner, M. (2018). Recent insights into the pathogenesis of nonalcoholic fatty liver disease. Annu. Rev. Pathol. 13, 321–350.

Beer, H.D., Munding, C., Dubois, N., Mamie, C., Hohl, D., and Werner, S. (2002). The estrogen-responsive B box protein: a novel regulator of keratinocyte differentiation. J. Biol. Chem. 277, 20740–20749.

Bell, J.L., Malyukova, A., Holien, J.K., Koach, J., Parker, M.W., Kavallaris, M., Marshall, G.M., and Cheung, B.B. (2012). TRIM16 acts as an E3 ubiquitin ligase and can heterodimerize with other TRIM family members. PLoS One 7, e37470.

Brenner, C., Galluzzi, L., Kepp, O., and Kroemer, G. (2013). Decoding cell death signals in liver inflammation. J. Hepatol. 59, 583–594.

Cai, J., Zhang, X.J., and Li, H. (2018). Role of innate immune signaling in nonalcoholic fatty liver disease. Trends Endocrinol. Metab. 29, 712–722.

Cai, J., Xu, M., Zhang, X., and Li, H. (2019). Innate immune signaling in nonalcoholic fatty liver disease and cardiovascular diseases. Annu. Rev. Pathol. 14, 153–184.

Chauhan, S., Kumar, S., Jain, A., Ponpuak, M., Mudd, M.H., Kimura, T., Choi, S.W., Peters, R., Mandell, M., Bruun, J.A., et al. (2016). TRIMs and galectins globally cooperate and TRIM16 and galectin-3 co-direct autophagy in endomembrane damage homeostasis. Dev. Cell 39, 13–27.

Chen, D.L., Shen, D.Y., Han, C.K., and Tian, Y. (2019a). LncRNA MEG3 aggravates palmitate-induced insulin resistance by regulating miR-185-5p/Egr2 axis in hepatic cells. Eur. Rev. Med. Pharmacol. Sci. 23, 5456–5467.

Chen, Z., Yu, Y., Cai, J., and Li, H. (2019b). Emerging molecular targets for treatment of nonalcoholic fatty liver disease. Trends Endocrinol. Metab. 30, 903–914.

Cheung, B.B., Koach, J., Tan, O., Kim, P., Bell, J.L., D'Andreti, C., Sutton, S., Malyukova, A., Sekyere, E., Norris, M., et al. (2012). The retinoid signalling molecule, TRIM16, is repressed during squamous cell carcinoma skin carcinogenesis in vivo and reduces skin cancer cell migration in vitro. J. Pathol. 226, 451–462.

Chokeshaiusaha, K., Puthier, D., Sananmuang, T., Olanratmanee, E.O., Nguyen, C., and Kedkovid, R. (2020). Differential DNA methylation analysis across the promoter regions using methylated DNA immunoprecipitation sequencing profiling of porcine loin muscle. Vet. World 13, 1113–1125.

Da Silva Morais, A., Lebrun, V., Abarca-Quinones, J., Brichard, S., Hue, L., Guigas, B., Viollet, B., and Leclercq, I.A. (2009). Prevention of steatohepatitis by pioglitazone: implication of adiponectin-dependent inhibition of SREBP-1c and inflammation. J. Hepatol. 50, 489–500.

Dar, A.C., and Shokat, K.M. (2011). The evolution of protein kinase inhibitors from antagonists to agonists of cellular signaling. Annu. Rev. Biochem. 80, 769–795.

Fan, H., Zhang, Y., Zhang, J., Yao, Q., Song, Y., Shen, Q., Lin, J., Gao, Y., Wang, X., Zhang, L., et al. (2020). Cold-inducible Klf9 regulates thermogenesis of brown and beige fat. Diabetes 69, 2603–2618.

Fatima, L.A., Campello, R.S., Barreto-Andrade, J.N., Passarelli, M., Santos, R.S., Clegg, D.J., and Machado, U.F. (2019). Estradiol stimulates adipogenesis and Slc2a4/GLUT4 expression via ESR1-mediated activation of CEBPA. Mol. Cell. Endocrinol. 498, 110447.

Fraiberg, M., and Elazar, Z. (2016). A TRIM16-Galactin3 complex mediates autophagy of damaged endomembranes. Dev. Cell 39, 1–2.

Friedman, S.L., Neuschwander-Tetri, B.A., Rinella, M., and Sanyal, A.J. (2018). Mechanisms of NAFLD development and therapeutic strategies. Nat. Med. 24, 908–922.

Grant, C.E., Bailey, T.L., and Noble, W.S. (2011). FIMO: scanning for occurrences of a given motif. Bioinformatics 27, 1017–1018.

Huck, I., Gunewardena, S., Espanol-Suner, R., Willenbring, H., and Apte, U. (2019). Hepatocyte nuclear factor 4 alpha activation is essential for termination of liver regeneration in mice. Hepatology 70, 666–681.

Hunter, T. (2007). The age of crosstalk: phosphorylation, ubiquitination, and beyond. Mol. Cell 28, 730–738.

Hwang, S., Wang, X., Rodrigues, R.M., Ma, J., He, Y., Seo, W., Park, S.H., Kim, S.J., Feng, D., and Gao, B. (2020). Protective and detrimental roles of p38alpha mitogen-activated protein kinase in different stages of nonalcoholic fatty liver disease. Hepatology 72, 873–891.

Ibrahim, S.H., Hirsova, P., and Gores, G.J. (2018). Non-alcoholic steatohepatitis pathogenesis: sublethal hepatocyte injury as a driver of liver inflammation. Gut 67, 963–972.

Inokuchi-Shimizu, S., Park, E.J., Roh, Y.S., Yang, L., Zhang, B., Song, J., Liang, S., Pimienta, M., Taniguchi, K., Wu, X., et al. (2014). TAK1-mediated autophagy and fatty acid oxidation prevent hepatosteatosis and tumorigenesis. J. Clin. Invest. 124, 3566–3578.

Jefferies, C., Wynne, C., and Higgs, R. (2011). Antiviral TRIMs: friend or foe in autoimmune and autoinflammatory disease? Nat. Rev. Immunol. *11*, 617–625.

Jena, K.K., Kolapalli, S.P., Mehto, S., Nath, P., Das, B., Sahoo, P.K., Ahad, A., Syed, G.H., Raghav, S.K., Senapati, S., et al. (2018). TRIM16 controls assembly and degradation of protein aggregates by modulating the p62-NRF2 axis and autophagy. EMBO J. *37*, e98358.

Ji, Y.X., Huang, Z., Yang, X., Wang, X., Zhao, L.P., Wang, P.X., Zhang, X.J., Alves-Bezerra, M., Cai, L., Zhang, P., et al. (2018). The deubiquitinating enzyme cylindromatosis mitigates nonalcoholic steatohepatitis. Nat. Med. *24*, 213–223.

Jian, C., Fu, J., Cheng, X., Shen, L.J., Ji, Y.X., Wang, X., Pan, S., Tian, H., Tian, S., Liao, R., et al. (2020). Low-dose sorafenib acts as a mitochondrial uncoupler and ameliorates nonalcoholic steatohepatitis. Cell Metab. *31*, 892–908.e11.

Jiang, M.S., Tang, Q.Q., McLenithan, J., Geiman, D., Shillinglaw, W., Henzel, W.J., and Lane, M.D. (1998). Derepression of the C/EBPalpha gene during adipogenesis: identification of AP-2alpha as a repressor. Proc. Natl. Acad. Sci. U. S. A. *95*, 3467–3471.

Joazeiro, C.A., and Weissman, A.M. (2000). Ring finger proteins: mediators of ubiquitin ligase activity. Cell *102*, 549–552.

Kim, D., Langmead, B., and Salzberg, S.L. (2015). HISAT: a fast spliced aligner with low memory requirements. Nat. Methods *12*, 357–360.

Kim, P.Y., Tan, O., Liu, B., Trahair, T., Liu, T., Haber, M., Norris, M.D., Marshall, G.M., and Cheung, B.B. (2016). High TDP43 expression is required for TRIM16-induced inhibition of cancer cell growth and correlated with good prognosis of neuroblastoma and breast cancer patients. Cancer Lett *374*, 315–323.

Kleiner, D.E., Brunt, E.M., Van Natta, M., Behling, C., Contos, M.J., Cummings, O.W., Ferrell, L.D., Liu, Y.C., Torbenson, M.S., Unalp-Arida, A., et al. (2005). Design and validation of a histological scoring system for nonalcoholic fatty liver disease. Hepatology *41*, 1313–1321.

Kodama, T., Yi, J., Newberg, J.Y., Tien, J.C., Wu, H., Finegold, M.J., Kodama, M., Wei, Z., Tamura, T., Takehara, T., et al. (2018). Molecular profiling of nonalcoholic fatty liver disease-associated hepatocellular carcinoma using SB transposon mutagenesis. Proc. Natl. Acad. Sci. U. S. A. *115*, E10417–E10426.

Lawan, A., and Bennett, A.M. (2017). Mitogen-activated protein kinase regulation in hepatic metabolism. Trends Endocrinol. Metab. *28*, 868–878.

Li, H., Handsaker, B., Wysoker, A., Fennell, T., Ruan, J., Homer, N., Marth, G., Abecasis, G., and Durbin, R.; 1000 Genome Project Data Processing Subgroup (2009). The Sequence Alignment/Map format and SAMtools. Bioinformatics *25*, 2078–2079.

Liu, D., Zhang, P., Zhou, J., Liao, R., Che, Y., Gao, M.M., Sun, J., Cai, J., Cheng, X., Huang, Y., et al. (2020). TNFAIP3 interacting protein 3 overexpression suppresses nonalcoholic steatohepatitis by blocking TAK1 activation. Cell Metab. *31*, 726–740.e8.

Love, M.I., Huber, W., and Anders, S. (2014). Moderated estimation of fold change and dispersion for RNA-seq data with DESeq2. Genome Biol. *15*, 550.

Lu, L., Ye, X., Yao, Q., Lu, A., Zhao, Z., Ding, Y., Meng, C., Yu, W., Du, Y., and Cheng, J. (2018). Egr2 enhances insulin resistance via JAK2/STAT3/SOCS-1 pathway in HepG2 cells treated with palmitate. Gen. Comp. Endocrinol. *260*, 25–31.

Marshall, G.M., Bell, J.L., Koach, J., Tan, O., Kim, P., Malyukova, A., Thomas, W., Sekyere, E.O., Liu, T., Cunningham, A.M., et al. (2010). TRIM16 acts as a tumour suppressor by inhibitory effects on cytoplasmic vimentin and nuclear E2F1 in neuroblastoma cells. Oncogene *29*, 6172–6183.

Michelotti, G.A., Machado, M.V., and Diehl, A.M. (2013). NAFLD, NASH and liver cancer. Nat. Rev. Gastroenterol. Hepatol. *10*, 656–665.

Mihaly, S.R., Ninomiya-Tsuji, J., and Morioka, S. (2014). TAK1 control of cell death. Cell Death Differ *21*, 1667–1676.

Moon, S.H., Huang, C.H., Houlihan, S.L., Regunath, K., Freed-Pastor, W.A., Morris, J.P.t., Tschaharganeh, D.F., Kastenhuber, E.R., Barsotti, A.M., Culp-Hill, R., et al. (2019). p53 represses the mevalonate pathway to mediate tumor suppression. Cell *176*, 564–580.e19.

Moravcová, A., Červinková, Z., Kučera, O., Mezera, V., Rychtrmoc, D., and Lotková, H. (2015). The effect of oleic and palmitic acid on induction of steatosis and cytotoxicity on rat hepatocytes in primary culture. Physiol. Res. *64*, S627–S636.

Munding, C., Keller, M., Niklaus, G., Papin, S., Tschopp, J., Werner, S., and Beer, H.D. (2006). The estrogen-responsive B box protein: a novel enhancer of interleukin-1beta secretion. Cell Death Differ *13*, 1938–1949.

Nagai, H., Noguchi, T., Homma, K., Katagiri, K., Takeda, K., Matsuzawa, A., and Ichijo, H. (2009). Ubiquitin-like sequence in ASK1 plays critical roles in the recognition and stabilization by USP9X and oxidative stress-induced cell death. Mol. Cell *36*, 805–818.

Ninomiya-Tsuji, J., Kajino, T., Ono, K., Ohtomo, T., Matsumoto, M., Shiina, M., Mihara, M., Tsuchiya, M., and Matsumoto, K. (2003). A resorcylic acid lactone, 5Z-7-oxozeaenol, prevents inflammation by inhibiting the catalytic activity of TAK1 MAPK kinase kinase. J. Biol. Chem. *278*, 18485–18490.

Nisole, S., Stoye, J.P., and Saïb, A. (2005). TRIM family proteins: retroviral restriction and antiviral defence. Nat. Rev. Microbiol. *3*, 799–808.

Noureddin, M., Vipani, A., Bresee, C., Todo, T., Kim, I.K., Alkhouri, N., Setiawan, V.W., Tran, T., Ayoub, W.S., Lu, S.C., et al. (2018). NASH leading cause of liver transplant in women: updated analysis of indications for liver transplant and ethnic and gender variances. Am. J. Gastroenterol. *113*, 1649–1659.

Pertea, M., Pertea, G.M., Antonescu, C.M., Chang, T.C., Mendell, J.T., and Salzberg, S.L. (2015). StringTie enables improved reconstruction of a transcriptome from RNA-seq reads. Nat. Biotechnol. *33*, 290–295.

Ren, X., Yu, J., Guo, L., and Ma, H. (2020). TRIM16 protects from OGD/R-induced oxidative stress in cultured hippocampal neurons by enhancing Nrf2/ARE antioxidant signaling via downregulation of Keap1. Exp. Cell Res. *391*, 111988.

Ricchi, M., Odoardi, M.R., Carulli, L., Anzivino, C., Ballestri, S., Pinetti, A., Fantoni, L.I., Marra, F., Bertolotti, M., Banni, S., et al. (2009). Differential effect of oleic and palmitic acid on lipid accumulation and apoptosis in cultured hepatocytes. J. Gastroenterol. Hepatol. *24*, 830–840.

Sanyal, A.J. (2019). Past, present and future perspectives in nonalcoholic fatty liver disease. Nat. Rev. Gastroenterol. Hepatol. *16*, 377–386.

Schuster, S., Cabrera, D., Arrese, M., and Feldstein, A.E. (2018). Triggering and resolution of inflammation in NASH. Nat. Rev. Gastroenterol. Hepatol. *15*, 349–364.

Song, M.J., and Malhi, H. (2019). The unfolded protein response and hepatic lipid metabolism in non alcoholic fatty liver disease. Pharmacol. Ther. *203*, 107401.

Subramanian, A., Tamayo, P., Mootha, V.K., Mukherjee, S., Ebert, B.L., Gillette, M.A., Paulovich, A., Pomeroy, S.L., Golub, T.R., Lander, E.S., et al. (2005). Gene set enrichment analysis: a knowledge-based approach for interpreting genome-wide expression profiles. Proc. Natl. Acad. Sci. U. S. A. *102*, 15545–15550.

Takeda, K., Noguchi, T., Naguro, I., and Ichijo, H. (2008). Apoptosis signal-regulating kinase 1 in stress and immune response. Annu. Rev. Pharmacol. Toxicol. *48*, 199–225.

Walter, D., Schmich, K., Vogel, S., Pick, R., Kaufmann, T., Hochmuth, F.C., Haber, A., Neubert, K., McNelly, S., von Weizsäcker, F., et al. (2008). Switch from type II to I Fas/CD95 death signaling on in vitro culturing of primary hepatocytes. Hepatology *48*, 1942–1953.

Wang, P.X., Ji, Y.X., Zhang, X.J., Zhao, L.P., Yan, Z.Z., Zhang, P., Shen, L.J., Yang, X., Fang, J., Tian, S., et al. (2017). Targeting CASP8 and FADD-like apoptosis regulator ameliorates nonalcoholic steatohepatitis in mice and nonhuman primates. Nat. Med. *23*, 439–449.

Wang, D., Tai, P.W.L., and Gao, G. (2019). Adeno-associated virus vector as a platform for gene therapy delivery. Nat. Rev. Drug Discov. *18*, 358–378.

Winston, J.T., Strack, P., Beer-Romero, P., Chu, C.Y., Elledge, S.J., and Harper, J.W. (1999). The SCFbeta-TRCP-ubiquitin ligase complex associates specifically with phosphorylated destruction motifs in IkappaBalpha and beta-catenin and stimulates IkappaBalpha ubiquitination in vitro. Genes Dev. *13*, 270–283.

Cell Metabolism
Article

Wree, A., Broderick, L., Canbay, A., Hoffman, H.M., and Feldstein, A.E. (2013). From NAFLD to NASH to cirrhosis-new insights into disease mechanisms. Nat. Rev. Gastroenterol. Hepatol. *10*, 627–636.

Wu, G., Xu, G., Schulman, B.A., Jeffrey, P.D., Harper, J.W., and Pavletich, N.P. (2003). Structure of a beta-TrCP1-Skp1-beta-catenin complex: destruction motif binding and lysine specificity of the SCF(beta-TrCP1) ubiquitin ligase. Mol. Cell *11*, 1445–1456.

Wu, T., Yoon, H., Xiong, Y., Dixon-Clarke, S.E., Nowak, R.P., and Fischer, E.S. (2020a). Targeted protein degradation as a powerful research tool in basic biology and drug target discovery. Nat. Struct. Mol. Biol. *27*, 605–614.

Wu, Y., Hu, Y., Wang, B., Li, S., Ma, C., Liu, X., Moynagh, P.N., Zhou, J., and Yang, S. (2020b). Dopamine uses the DRD5-ARRB2-PP2A signaling axis to block the TRAF6-mediated NF-κB pathway and suppress systemic inflammation. Mol. Cell *78*, 42–56.e6.

Xu, M., Liu, P.P., and Li, H. (2019). Innate immune signaling and its role in metabolic and cardiovascular diseases. Physiol. Rev. *99*, 893–948.

Yang, L., Inokuchi, S., Roh, Y.S., Song, J., Loomba, R., Park, E.J., and Seki, E. (2013). Transforming growth factor-beta signaling in hepatocytes promotes hepatic fibrosis and carcinogenesis in mice with hepatocyte-specific deletion of TAK1. Gastroenterology *144*, 1042–1054.e4.

Younossi, Z.M., Koenig, A.B., Abdelatif, D., Fazel, Y., Henry, L., and Wymer, M. (2016). Global epidemiology of nonalcoholic fatty liver disease-meta-analytic assessment of prevalence, incidence, and outcomes. Hepatology *64*, 73–84.

Younossi, Z., Tacke, F., Arrese, M., Chander Sharma, B., Mostafa, I., Bugianesi, E., Wai-Sun Wong, V., Yilmaz, Y., George, J., Fan, J., et al. (2019). Global perspectives on nonalcoholic fatty liver disease and nonalcoholic steatohepatitis. Hepatology *69*, 2672–2682.

STAR★METHODS

KEY RESOURCES TABLE

REAGENT or RESOURCE	SOURCE	IDENTIFIER
Antibodies		
anti-TRIM16, dil: 1/100	Santa Cruz	Cat#sc-398851
anti-CD11b, dil: 1/100	Boster	Cat#BM3925; RRID: AB_2832991
Goat anti-mouse IgG (H+L), dil:1/5000	Jackson	Cat#115-035-003; RRID: AB_10015289
Goat anti-rabbit IgG (H+L), dil:1/5000	Jackson	Cat#111-035-003; RRID: AB_2313567
Alexa Flour 568 goat anti-rabbit IgG (H+L), dil:1/200	Invitrogen	Cat#A11036; RRID: AB_10563566
Alexa Flour 488 goat anti-rabbit IgG (H+L), dil:1/200	Invitrogen	Cat#A11034; RRID: AB_2576217
Alexa Flour 488 goat anti-mouse IgG (H+L), dil:1/200	Invitrogen	Cat#A11029; RRID: AB_2534088
Alexa Flour 568 donkey anti-goat IgG (H+L), dil:1/200	Invitrogen	Cat#A11057; RRID: AB_2534104
anti-phospho-TAK1 (Thr184/187), dil:1/1000	Cell Signaling Technology	Cat#4531; RRID: AB_390772
anti-TAK1, dil:1/1000	Cell Signaling Technology	Cat#4505; RRID: AB_490858
anti-phospho-JNK1/2 (Thr183/Tyr185), dil:1/1000	Cell Signaling Technology	Cat#4668; RRID: AB_823588
anti-JNK1/2, dil:1/1000	Cell Signaling Technology	Cat#9258; RRID: AB_2141027
anti-phospho-p38 (Thr180/Tyr182), dil:1/1000	Cell Signaling Technology	Cat#4511; RRID: AB_2139682
anti-p38, dil:1/1000	Cell Signaling Technology	Cat#9212; RRID: AB_330713
anti-phospho-ERK1/2 (Thr202/Thr204), dil:1/1000	Cell Signaling Technology	Cat#4370; RRID: AB_2315112
anti- ERK1/2, dil:1/1000	Cell Signaling Technology	Cat#4695; RRID: AB_390779
anti-HA, dil:1/1000	Cell Signaling Technology	Cat#3724; RRID: AB_1549585
anti-Ub, dil:1/1000	Cell Signaling Technology	Cat#3933; RRID: AB_2180538
anti-Flag, dil:1/1000	Cell Signaling Technology	Cat#14793; RRID: AB_2572291
anti-HA, dil:1/500	MBL	Cat#M180-3; RRID: AB_10951811
anti-Flag, dil:1/500	MBL	Cat#M185; RRID: AB_10950447
anti-Myc, dil:1/500	MBL	Cat#M047-3; RRID: AB_591112
anti-Ub (K48), dil:1/1000	Abclonal	Cat#A18163; RRID: AB_2861948
anti-β-Actin, dil:1/50000	Abclonal	Cat#AC026; RRID: AB_2768234
anti-Myeloperoxidase, dil:1/500	Abcam	Cat#Ab45977; RRID: AB_944318
anti-F4/80, dil:1/500	Servicebio	Cat#GB11027; RRID: AB_2814687
Mouse Control IgG, dil:1/500	Abclonal	Cat#AC011; RRID: AB_2770414
Rabbit Control IgG, dil:1/500	Abclonal	Cat#AC005; RRID: AB_2771930
Chemicals, peptides, and recombinant proteins		
5Z-7-Oxozeaenol	Sigma-Aldrich	Cat#O9890
Oil Red O	Sigma-Aldrich	Cat#O0625
Picrosirius Red	Hede Biotechnology	Cat#26357-02
Fetal Bovine Serum (FBS)	Bio-One Biotechnology	Cat#F05-001-B160216
Penicillin-Streptomycin	GIBCO	Cat#15140-122
Palmitic acid (PA)	Sigma-Aldrich	Cat#P0500
Oleic acid (OA)	Sigma-Aldrich	Cat#O-1008
BSA, essentially fatty acid free	Equitech Bio	Cat#BAH66-0100
MG132	Selleck	Cat#S2619
Liver Perfusion Medium	Thermo Fisher Scientific	Cat#17701-038

(Continued on next page)

Cell Metabolism
Article

⟋ CellPress

Continued

REAGENT or RESOURCE	SOURCE	IDENTIFIER
Liver Digestion Medium	Thermo Fisher Scientific	Cat#17701-034
Nile Red	Fanbo Biochemicals	Cat#22190
Passive Lysis 5X Buffer	Promega	Cat#E1941
PacI	NEB	Cat#R0547L
Polyethyleneimine (PEI)	Polysciences	Cat#24765-1
Trizol	Sigma-Aldrich	Cat#T9424
Insulin	Thermo Fisher Scientific	Cat#12585-014
Polybrene	Millipore	Cat#TR-1003-G
Formalin	Thermo Fisher Scientific	Cat#23-305-510
RIPA buffer	Beyotime Biotechnology	Cat#P0013E
Triton X-100	Sigma-Aldrich	Cat#T8787
Trypsin	GIBCO	Cat#27250-018
DAPI	Invitrogen	Cat#S36939
PMSF	Beyotime Biotechnology	Cat#ST506
SYBR Green PCR Master Mix	Roche	Cat#04887352001
Critical commercial assays		
pAd/CMV/V5-DEST Gateway kit	Invitrogen	Cat#V493-20
DNA Purification Kit	Beyotime Biotechnology	Cat#D0033
LDH cytotoxicity assay kit	Beyotime Biotechnology	Cat#C0017
ChIP Assay Kit	Beyotime Biotechnology	Cat#P2078
BCA protein assay kit	Thermo Fisher Scientific	Cat#23225
ECL kit	Bio-Rad	Cat#170-5061
LabAsssay Cholesterol	Wako	Cat#294-65801
LabAsssay Triglyceride	Wako	Cat#290-63701
Deposited data		
RNA-seq data of L02 hepatocytes treated with PAOA	This paper, NCBI SRA	PRJNA726826
RNA-seq data of murine primary hepatocytes treated with PAOA	This paper, NCBI SRA	PRJNA726846
RNA-seq data of murine primary hepatocytes transfected with Ad*Trim16*	This paper, NCBI SRA	PRJNA726822
RNA-seq data of *Trim16*-HKO mice fed with HFHC diet	This paper, NCBI SRA	PRJNA726824
Ubiquitinomic data of L02 hepatocytes transfected with Flag-TRIM16 plasmid	This paper, PRIDE	PXD025772
Experimental models: Cell lines		
Human: L02 (HL-7702)	Type Culture Collection of the Chinese Academy of Sciences	Cat#GNHu 6
Human: HEK293T	Type Culture Collection of the Chinese Academy of Sciences	Cat#GNHu17
Human: HEK293	Type Culture Collection of the Chinese Academy of Sciences	Cat#GNHu43
Mouse: primary hepatocytes	This paper	N/A
Experimental models: Organisms/strains		
albumin-Cre transgenic mice	Jackson Laboratory	Cat#003574
TRIM16 hepatocyte-specific knockout mice (*Trim16*-HKO)	This paper	N/A
TRIM16 hepatocyte-specific overexpression mice (*Trim16*-OE)	This paper	N/A
C57BL/6	Vital River	N/A

(Continued on next page)

Continued

REAGENT or RESOURCE	SOURCE	IDENTIFIER
Oligonucleotides		
Primers of plasmids for luciferase reporting assay, see Table S1	This paper	N/A
Primers of TRIM16 promoter segments for ChIP PCR assay, see Table S2	This paper	N/A
sgRNA target sequences for knockout mice construction, see Table S3	This paper	N/A
Primers for genotyping the transgenic mice, see Table S4	This paper	N/A
Primers for overexpressing plasmids construction, see Table S5	This paper	N/A
Primers for lentiviral and adenoviral plasmids construction, see Table S6	This paper	N/A
Primers for qPCR, see Table S7	This paper	N/A
Software and algorithms		
HISAT2 2.1.0	Kim et al. (2015)	https://ccb.jhu.edu/software/hisat2/index.shtml
SAMtools 1.4	Li et al. (2009)	https://github.com/samtools/samtools
StringTie 1.3.3b	Pertea et al. (2015)	http://ccb.jhu.edu/software/stringtie/
DESeq2 1.2.10	Love et al. (2014)	https://bioconductor.org/packages/release/bioc/html/DESeq2.html
FIMO	Grant et al. (2011)	http://meme-suite.org/tools/fimo
SPSS statistics 19.0	IBM Corp	https://www.ibm.com/cn-zh/products/spssstatistics
GraphPad Prism 7	Graphpad Software	https://www.graphpad.com/
FIJI running ImageJ, version 1.52p	ImageJ	https://imagej.nih.gov/ij/
GSEA 3.0	Subramanian et al. (2005)	http://software.broadinstitute.org/gsea/index.jsp
Other		
Mouse high fat diet	Huafukang Bioscience	Cat#D12492
Mouse high fat high cholesterol diet	TrophicDiet	Cat#TP26304
Mouse normal chow diet	Huafukang Bioscience	Cat#H1025
PVDF membranes	Millipore	Cat#IPVH00010
GloMax 20/20 Luminometer	Promega	Cat#E5311

RESOURCE AVAILABILITY

Lead Contact
Further information and requests for resources and reagents should be directed to the Lead Contact, Lin Wang (fierywang@163.com)

Materials availability
This study did not generate new unique reagents.

Data and code availability
All RNA sequencing data generated in this study have been deposited to the National Center for Biotechnology Information (NCBI) Sequence Read Archive (SRA) database. And the ubiquitinomic data have been deposited to the ProteomeXchange Consortium via the proteomics identification (PRIDE) partner repository. The accession numbers of the data mentioned above are listed in the key resources table.

EXPERIMENTAL MODEL AND SUBJECT DETAILS

Mice
C57BL/6J mice (8-10 weeks of age) were purchased from Vital River, Beijing, China and housed under pathogen-free conditions in a temperature-controlled environment at 22-24°C under a 12-hour light/dark cycle. Mice had free access to food and water and

Cell Metabolism
Article

🔗 **CellPress**

were in generally good health before HFD or HFHC administration. After necessary acclimatization, the imported C57BL/6J mice were used in experiments. The *Trim16*-Flox littermates were used as the control of *Trim16*-HKO mice. A randomization process was performed in grouping mice. Male mice were fed a HFD (protein, 20%; fat, 60%; carbohydrates, 20%; D12942; HUAFUKANG Bioscience; Beijing, China) for 24 weeks to establish a fatty liver model. To establish the NASH model, male mice were fed a HFHC (protein, 14%; fat, 42%; carbohydrates, 44%; cholesterol, 0.2%; TP 26304; Trophic Diet; Nantong, China) diet for 16 weeks. The corresponding control group mice were fed normal chow (NC: protein, 18.3%; fat, 10.2%; carbohydrates, 71.5%; H1025; HUA-FUKANG Bioscience; Beijing, China). For TAK1 inhibition in vivo, the TAK1 inhibitor 5Z-7-oxozeaenol (5Z-7-ox; O9890-1 MG; Sigma-Aldrich; St. Louis, MO, USA; 5 mg/kg) was intraperitoneally injected into *Trim16*-HKO and *Trim16*-Flox mice. All animal experiments were approved by the Animal Care and Use Committee of Fourth Military Medical University and the Institutional Animal Care and Use Committee of the Institute of Model Animals of Wuhan University. The animals received humane care according to the criteria outlined in the Guide for the Care and Use of Laboratory Animals prepared by the National Academy of Sciences and published by the National Institutes of Health.

Primary hepatocytes
A collagenase perfusion and gradient centrifugation method was used to isolate primary hepatocytes from 6- to 8-week-old male C57BL/6 mice as previously described (Walter et al., 2008). In brief, mice were anesthetized and perfused with Liver Perfusion Medium (17701-038; Thermo Fisher Scientific; Waltham, MA, USA) and then Liver Digestion Medium (17701-034; Thermo Fisher Scientific; Waltham, MA, USA) via the portal vein. Then, the liver was acquired and filtered through a 100 μm cell strainer. After that, the cells were centrifuged at 50×g for 1 min and then cultured with DMEM containing 10% FBS (F05-001-B160216; Bio-One Biotechnology; Guangzhou, China) and 1% penicillin-streptomycin (15140-122; Gibco by Invitrogen; Carlsbad, CA, USA) at 37°C as described before.

Cell lines
The human hepatocyte L02, human embryonic kidney 293 and 293T cell lines were purchased from the Cell Bank of the Type Culture Collection of the Chinese Academy of Sciences, Shanghai, China. Mouse primary hepatocytes, L02, HEK293 and HEK293T cell lines were cultured in a 5% CO2 incubator. All cells were cultured in Dulbecco's modified Eagle's medium (DMEM) supplemented with 10% FBS and 1% penicillin-streptomycin. All the cell lines were examined for mycoplasma contamination, and the results were negative. To establish a hepatic steatosis model in vitro, human hepatocyte L02 cells and mouse primary hepatocytes were stimulated with palmitic acid (PA; 0.5 mM; P0500; Sigma-Aldrich; St. Louis, MO, USA) and oleic acid (OA; 1.0 mM; O-1008; Sigma-Aldrich; St. Louis, MO, USA) (dissolved in 0.5% fatty acid–free BSA) at the indicated concentrations for 12-16 hours. For the control group, cells were stimulated with fatty acid-free BSA (0.5%; BAH66-0100; Equitech Bio; Kerrville, TX, USA). For TAK1 inhibitory experiment, hepatocytes were treated with 5Z-7-oxozeaenol (O9890-1 MG; Sigma-Aldrich; St. Louis, MO, USA) at 2 μM concentration to inhibit TAK1 activation. To determine whether TRIM16 facilitates the proteasomal degradation of p-TAK1, the cells were treated with 25mM of MG132 (S2619; Selleck; Houston, TX, USA) for 12 hours.

Human liver samples
From January 2018 to June 2019, 20 individuals with NASH undergoing hepatic surgery at the Department of Hepatobiliary Surgery, Xijing Hospital of the Fourth Military Medical University were enrolled to this study. All the individuals enrolled in this study were excluded of drug abuse, hepatitis virus infection or excessive alcohol consumption (> 140 g for men or > 70 g for women, per week). Two pathologists independently used the NASH-CRN scoring system (Kleiner et al., 2005) to evaluate the NAFLD activity score (NAS) in a blinded fashion. The non-NASH samples possessed an NAS of 0. The NASH samples possessed a NAS > 4, or NAS at 3-4 but exhibiting fibrosis. Human sample collection and application were conducted under the supervision of the ethics committee of Xijing Hospital of Fourth Military Medical University and adhered to the principles of the Declaration of Helsinki. All individuals have signed an informed consent for the use of clinical specimens in the present study.

METHOD DETAILS

Generation of genetically modified mice
Trim16-Flox mice were generated using a CRISPR/Cas9 system in the C57BL/6 background. Two single guide RNAs (sgRNA1 and sgRNA2, listed in Table S3) targeting *Trim16* introns 3 and 4 were designed by an online CRISPR design tool (http://chopchop.cbu.uib.no/). Targeting constructs were generated by introducing the loxp-flanked *Trim16* exon 4 into the left and right homology arms (906 bp & 644 bp) of HMEJ. The genes of the *Trim16*-Flox mice were amplified by PCR analysis with the primer pairs P4 and P5. To confirm that the Flox allele was functional, we used genomic DNA for in vitro Cre-loxP-mediated recombination. Primer pairs P1 and P5, as well as P3 and P4, were used to detect the deletion product and the circle product, respectively. All products were confirmed by sequencing. The primers (P1 to P6) are listed in Table S4. Founder mice were mated with C57BL/6J female mice to obtain homozygous *Trim16*-Flox mice. Hepatocyte-specific Trim16-knockout (*Trim16*-HKO) mice were generated by mating *Trim16*fl/fl mice with albumin-Cre transgenic mice (003574; Jackson Laboratory; Bar Harbor, ME, USA).

Mouse metabolic and liver function assays
Body weight and fasting blood glucose (FBG) levels were assessed in mice every 4 weeks. For GTT and ITT assays, the mice were fasted for 6 hours, and blood glucose levels were measured at the indicated time points after injection with 1 g/kg glucose or 0.75 IU/kg insulin (12585-014; Thermo Fisher Scientific; Waltham, MA, USA) via the tail vein. Then, the conventional trapezoid rule was used to calculate the areas under the curve. GTT tests were performed in the model at 22 weeks of HFD feeding and at 14 weeks of HFHC feeding. ITT tests were carried out in the model at 23 weeks of HFD feeding and at 15 weeks of HFHC feeding. Serum triglyceride (TG), total cholesterol (TC), alanine aminotransferase (ALT) and aspartate aminotransferase (AST) concentrations were measured by an ADVIA 2400 Chemistry System Analyzer (Siemens, Tarrytown, NY, USA), according to the manufacturer's instructions.

Lipid analysis
Commercial kits were used to measure the hepatic TG and TC contents (290-63701 for TG, 294-65801 for TC; Wako; Tokyo, Japan), according to the manufacturer's instructions.

Histopathological analysis
Liver tissues were fixed with 10% formaldehyde overnight. Paraffin-embedded and OCT-embedded liver sections were used for H&E staining and Oil Red O (O0625; Sigma-Aldrich; St. Louis, MO, USA) staining, respectively. Liver fibrosis was assessed by picrosirius red (PSR; 26357-02; Hede Biotechnology; Beijing, China) staining, and the histological images were acquired with a light microscope (Olympus; Tokyo, Japan).

Immunofluorescence staining and confocal microscopy
To perform CD11b and F4/80 immunofluorescence staining, paraffin sections of liver tissues were first labeled with an anti-CD11b or anti-F4/80 primary antibody overnight at 4°C and then incubated with a fluorophore-conjugated secondary antibody (Alex Flour 568 goat anti-Rabbit IgG (H+L); A11036; Invitrogen; Carlsbad, CA, USA). A fluorescence microscope (Olympus; Tokyo, Japan) was used to acquire immunofluorescence images. For coverslip staining, L02 hepatocytes transfected with the indicated plasmids were incubated with mouse anti-Flag and rabbit anti-HA tag antibodies at 4°C and were then labeled with fluorophore-conjugated secondary antibodies. Nuclei in all images were stained with DAPI (S36939; Invitrogen; Carlsbad, CA, USA). Images were acquired with a confocal laser scanning microscope (TCS SP8; Leica; Wetzler, Germany). All antibodies used in this study are listed in the key resources table.

Cellular Nile Red staining
For Nile Red staining, L02 cells and mouse primary hepatocytes were treated with PAOA for 0, 12 or 24h. Then, the cells were fixed with 4% paraformaldehyde and stained with Nile Red (1 μM in PBS; 22190; Fanbo Biochemicals; Beijing, China). Lipid accumulation were visualized and quantified by a laser scanning confocal microscope (TCS SP8; Leica; Wetzler, Germany) or a high-content analysis system (Operetta CLS; Waltham, MA, USA).

LDH analysis
Commercial kits (C0017, Beyotime Biotechnology; Shanghai, China) were used to measure the LDH contents in PAOA-treated L02 hepatocytes and mouse primary hepatocytes, according to the manufacturer's protocol.

Dual-luciferase reporter assay
L02 hepatocytes were seeded in 24-well culture plates at 8×10^4 cells per well. Then the cells were transfected with the luciferase report plasmid containing TRIM16 promoter (200 ng) together with the plasmids overexpressing different transcription factors or the control plasmid (200 ng) in the presence of pRLTK (Renilla luciferase, 50 ng). The primers used for the construction of the plasmids mentioned above are listed in Table S1. After twenty-four hours of transfection, the cells were lysed (E1941; Promega; WI, USA) and the luciferase activity was measured using the Dual-Glo Luciferase Assay system (GloMax 20/20 Luminometer; E5311; Promega; WI, USA).

Plasmid construction and viral infection
All full-length, truncated or mutant TAK1 and TRIM16 were inserted into the pcDNA5 vector via PCR-based cloning. The shuttle plasmid pENTR-U6-CMV-flag-T2A-EGFP and ViraPower Adenoviral Expression System (V493-20; Invitrogen; Carlsbad, CA, USA) were used to generate mouse TRIM16-overexpressing or TRIM16-knockdown adenoviral vectors. The recombinant adenoviral vector was linearized by PacI (R0547L; NEB; MA, USA) before cotransfection into 293 cells with polyethyleneimine (PEI; 24765-1; Polysciences; Warrington, UK) transfection reagent. Cells were harvested after 6-7 days to assess the initial virus. The adenovirus was amplified by infecting 293 producer cells with the crude viral lysate, and the TRIM16 adenovirus was purified by cesium chloride density gradient centrifugation. Then, the titer was measured by the 50% tissue culture infective dose (TCID50) method. Mouse primary hepatocytes were infected with adenovirus at a multiplicity of infection (MOI) of 50. The primer sequences used for plasmid construction are listed in Tables S5 and S6. For in vivo assays, adeno-associated virus 8 expressing the mouse TRIM16 protein or GFP (purchased from Vigenebio; Shandong, China) was injected intraperitoneally the 8th week after HFHC consumption as previously described (Huck et al., 2019). For the generation of *Trim16*-OE mice, a Sleeping Beauty (SB) transposase system was applied

Cell Metabolism
Article

CellPress

as previously described (Kodama et al., 2018; Moon et al., 2019). In brief, a liver-specific pT3 plasmid carrying *Trim16* (pT3-alb-3xflag-h-*Trim16*) (30 μg per mouse) and the SB100X transposase plasmid (2 μg per mouse) were injected into mouse livers via the tail vein.

Quantitative PCR analysis
Total RNA was extracted with Trizol reagent (T9424; Sigma-Aldrich; St. Louis, MO, USA), and quantitative PCR (qPCR) assays were performed with SYBR Green PCR Master Mix (04887352001, Roche; Basel, BS, Switzerland) in a Real-Time PCR System (LightCycler 480 Instrument II, Roche; Basel, BS, Switzerland), according to the manufacturer's instructions. β-actin was used as the housekeeping gene. The primers used are listed in Table S7.

Western blot analysis
To perform western blot analysis, tissues and cells were isolated and lysed with RIPA lysis buffer (P0013E; Beyotime Biotechnology; Shanghai, China). Total protein was then quantified using a BCA kit (23225; Thermo Fisher Scientific; Waltham, MA, USA). Then, equal quantities of the indicated protein were separated by 10% SDS-PAGE and transferred to PVDF membranes (IPVH00010; Millipore; Billerica, MA, USA). The PVDF membranes with proteins were blocked with 5% skim milk in TBST, incubated with the indicated primary antibodies overnight at 4°C and incubated with HRP-conjugated secondary antibodies. The proteins were then detected using an ECL kit (170-5061; Bio-Rad; Hercules, CA, USA) and visualized in a ChemiDoc MP Imaging System (Bio-Rad; Hercules, CA, USA). The antibodies used are listed in the key resources table.

Immunoprecipitation assays
Immunoprecipitation (IP) assays were performed as described previously (Wang et al., 2017). Briefly, 293T and L02 cells transfected with the indicated plasmids were lysed with IP lysis buffer (20 mM Tris-HCl, pH 7.4; 150 mM NaCl; 1 mM EDTA; and 1% NP-40) containing an inhibitor cocktail (04693132001; Roche; Basel, BS, Switzerland). After centrifugation (12,000 g for 10 min), each sample was incubated with protein A/G agarose beads (11719394001, 11719386001; Roche; Basel, BS, Switzerland) and the indicated anti-tag antibodies overnight at 4°C. For endogenous IP, cells were incubated with the indicated primary antibody. The beads were then washed with IP lysis buffer for 4 times. And after centrifugation, the protein was boiled with SDS loading buffer for 10 min. Finally, western blotting was performed as mentioned before.

Ubiquitination assays
Liver tissue or L02 hepatocytes transfected with the indicated plasmids were lysed in 100 μl 10 % SDS lysis buffer and then denatured by heating at 95°C for 10 min. Then, 0.9 ml IP lysis buffer (20 mM Tris-HCl, pH 7.4; 150 mM NaCl; 1 mM EDTA; and 1% NP-40) were added to the lysates. After sonication and centrifugation (12,000 g for 10 min), the supernatants were incubated with anti-tag or antibody of target proteins as well as protein A/G agarose beads (11719394001, 11719386001; Roche; Basel, BS, Switzerland) at 4 °C for 3 h. The beads were then washed with IP lysis buffer for three times. And after centrifugation, the protein was boiled with SDS loading buffer for 10 min. Finally, western blotting was performed as mentioned before.

Chromatin Immunoprecipitation (ChIP)
L02 hepatocytes transfected with the EGR2 overexpressing plasmid were cross-linked with 1% formaldehyde for 5 min at 37 °C and were stopped by 0.125 M glycine for 10 min at room temperature. The hepatocytes were washed twice with cold PBS containing PMSF (ST506; Beyotime Biotechnology; Shanghai, China) and harvested in SDS Lysis buffer from a ChIP Assay Kit (P2078; Beyotime Biotechnology; Shanghai, China). Then, the Bioruptor Plus (Diagenode, Belgium) was used to sonicate the sample (260 W, 25 times, 30 s on/60 s off) at 4 °C. Protein A+G Agarose/Salmon Sperm DNA were used to preclear the whole cell lysate for 30 min at 4 °C. After the 2 % input sample was extracted, the sample were divided equally and incubated with anti-Flag (M185; MBL; Nagoya, Japan) or control IgG antibody (AC011; ABclonal; Wuhan, China) overnight. Then, Protein A+G Agarose/Salmon Sperm DNA were added for 2 hour-incubation at 4 °C. Thereafter, the beads were washed sequentially with Low-Salt Immune Complex Wash Buffer, High-Salt Immune Complex Wash Buffer, LiCl Immune Complex Wash Buffer and TE Buffer (twice) for 5 min at 4 °C rotation. DNA-protein complexes were eluted with elution buffer (1% SDS and 0.1 M NaHCO$_3$) and de-crosslinked by adding 0.2 M NaCl and heating for 4 hours at 65 °C. Then, the proteins were digested with proteinase K for 1 hour at 45 °C, and the DNA segments were purified by a DNA Purification Kit (D0033; Beyotime Biotechnology; Shanghai, China) and used for qPCR reaction. The primers for ChIP-PCR are listed Table S2.

RNA-seq and data processing
To profile the gene expression differences, total RNA was extracted and then used to construct cDNA libraries. Single-end libraries were sequenced using BGISEQ 500 (MGI Tech; Shenzhen, China). The reads were mapped to Ensembl mouse (mm10/GRCm38)/human (hg38/GRCh38) reference genomes by HISAT2 software (version 2.1.0). Binary Alignment Map (BAM) files were generated by SAMtools (version 1.4). Fragments per kilobase of exon model per million mapped fragments (FPKM) values of genes were calculated by StringTie (version 1.3.3b). DESeq2 (version 1.2.10) was used for differential gene expression analysis. Genes with a fold change greater than 1.5 and corresponding adjusted *P value*s less than 0.05 were identified as DEGs.

Identification of candidate genes

To identify the genes that may influence NASH, we screened candidate genes using the following strategy: (1) The upregulated DEGs (log2FoldChange > $log_2(1.5)$, adjusted *P value*s< 0.05) of 4 pairwise comparisons (primary hepatocytes of mice with 0 h PAOA treatment vs primary hepatocytes of mice with 12 h PAOA treatment; primary hepatocytes of mice with 0 h PAOA treatment vs primary hepatocytes of mice with 24 h PAOA treatment; L02 cell lines with 0 h PAOA treatment vs L02 cell lines with 12 h PAOA treatment; L02 cell lines with 0 h PAOA treatment vs L02 cell lines with 24 h PAOA treatment) are intersected. (2) The downregulated DEGs (log2-FoldChange2 < $-log_2(1.5)$, adjusted *P value*s< 0.05) of 4 pairwise comparisons (primary hepatocytes of mice with 0 h PAOA treatment vs primary hepatocytes of mice with 12 h PAOA treatment; primary hepatocytes of mice with 0 h PAOA treatment vs primary hepatocytes of mice with 24 h PAOA treatment; L02 cell lines with 0 h PAOA treatment vs L02 cell lines with 12 h PAOA treatment; L02 cell lines with 0 h PAOA treatment vs L02 cell lines with 24 h PAOA treatment) are intersected. (3) The union of the screened upregulated DEGs and downregulated DEGs was then intersected with the union of the E3 ubiquitin ligase database and deubiquitinating enzymes (DUBs) database. (4) Finally, genes in the intersection of DEGs and E3 and DUBs were sorted by the average |log2FoldChange| in primary hepatocytes of mice and L02 cell lines, respectively.

Scanning of TRIM16 promoter-binding transcription factors

The FIMO (Find Individual Motif Occurrences) tool was used for scanning the transcription factors on TRIM16 promoter (Grant et al., 2011). Specifically, transcription factors targeted motifs on either strand of human or mouse TRIM16 promoter sequences were searched under the default screening condition (p-value < 10^{-4}). And 121 conservative motifs possessing q-value < 0.05 were selected, respectively. Then, 28 overlapping motifs on both human or mouse TRIM16 promoter, which matched 12 transcription factors, were identified. After analysis of the existing literature regarding these 12 transcription factors, 5 of them (ZNF384, ESR1, TFAP2A, EGR2 and KLF9) associated with lipid metabolism (Chen et al., 2019a; Chokeshaiusaha et al., 2020; Fan et al., 2020; Fatima et al., 2019; Jiang et al., 1998; Lu et al., 2018) were selected for further study.

Hierarchical clustering analysis

A hierarchical clustering analysis was performed to construct a phylogenetic tree of samples by the R function "hclust" using an unweighted average distance algorithm.

Gene set enrichment analysis (GSEA)

Each KEGG pathway or GO biological process term and involved genes were defined as a gene set, and GSEA was implemented with the Java GSEA (version 3.0) platform with the 'Signal2Noise' metric to generate a ranked list and a 'gene set' permutation type. Gene sets with FDR values < 0.25 were considered statistically significant.

KEGG pathway enrichment analysis

KEGG pathway enrichment analysis was performed using Fisher's exact test with our in-house R script. The KEGG pathway annotations were downloaded from the KEGG database. Pathways with a *P value* less than 0.05 were defined as significantly enriched pathways.

Mass spectrometry analysis

TRIM16 and its interacting protein were immunoprecipitated as described above in the IP assay. The proteins were subjected to liquid chromatography–tandem mass spectrometry (LC-MS/MS) analysis. The criteria for selecting the candidate molecules were as follows: 1) the candidates should be presented in the PAOA-treated group but be diminished in the BSA-treated group and 2) the number of unique peptides should be > 2.

Ubiquitinated proteome analysis

The ubiquitinated peptides were subjected to LC-MS/MS analysis. Label-free quantification was performed to compare the abundances of ubiquitinated peptides between the control and treatment samples, and Student's t-test was used to identify significant changes between controls and treatments. Ubiquitinated peptides with 1) fold changes > 1.5 and *P value*s < 0.05 or 2) quantified in only one group were considered to be differentially expressed ubiquitinated peptides.

QUANTIFICATION AND STATISTICAL ANALYSIS

All data were analyzed using appropriate statistical methods with SPSS software. Differences between 2 groups were evaluated using Student's t-test. For comparisons among multiple groups, one-way ANOVA followed by the Bonferroni post hoc test (for data showing homogeneity of variance) or Tamhane T2 post hoc test (for heteroscedastic data) was applied. A *P value* of less than 0.05 was considered statistically significant. All data are presented as the mean ± SD values, and the statistical methods used and the corresponding *P value*s for the data are shown following each figure legend. We determined sample size according to a previous study (Ji et al., 2018). We collected data from animal studies in a blinded manner. No data was excluded when conducting the final statistical analysis.